INVESTIGATING THE OPTICAL AND ELECTRICAL PROPERTIES OF Cu_2O AND ZnS: Al THIN FILMS FOR SOLAR CELL APPLICATIONS

OTIENO PHILIP JEREMIA (B.Ed. Sc)

I56/CE/22396/2010

A thesis submitted in partial fulfillment of the requirements for the award of the degree of Master of Science (Electronics and Instrumentation) in the School of Pure and Applied Sciences of Kenyatta University

NOVEMBER, 2019

DECLARATION

This thesis is my original work and has not been presented for the award of a degree or any other award in any other University

Otieno Philip Jeremia	**Signature**	**Date**
Department of Physics Kenyatta University	.....	6/11/2019

This thesis has been submitted for Examination with our approval as University Supervisors.

Dr. Njoroge W. K.	**Signature**	**Date**
Department of Physics Kenyatta University	.....	06/11/2019

Dr. Munji M. K.	**Signature**	**Date**
Department of Physics Kenyatta University	.....	6.11.2019

DEDICATION

This thesis is dedicated to my wife Florence, sons Jeremiah, Clement and my mother Silvia.

ACKNOWLEDGEMENTS

I am very grateful to my supervisors Dr. Walter Njoroge and Dr. Mathew Munji for their direction, pieces of advice and monitoring during the project. I also thank the Vice Chancellor of Kenyatta University, Prof. Paul Wainaina for the favourable learning environment he provided, which was of great benefit to this research. I also appreciate the members of staff, Department of Physics, Kenyatta University for their technical guidance during the research period. This project involved a lot of laboratory work, and I therefore acknowledge Mr. Otiato John, Chief Technician, Department of Physics, Maseno University, Mr. Mudimba Fredrick, Chief Technician, Department of Physics, Kenyatta University and Mr. Muthoka Boniface, Chief Technician, solid state physics laboratory, University of Nairobi, who availed for me and inducted me on how to use the required apparatus and machines. I also appreciate the teaching staff of Onjiko High school under the leadership of Mr. Ochiel Alfred for their encouragements and support during my studies. Much thanks goes to my family for their moral support throughout my studies. Special regards to my colleagues and friends Mr. Obare Peter and Nyakiti Kevin for their moral support.

TABLE OF CONTENTS

LIST OF TABLES

LIST OF FIGURES

SYMBOLS AND ABBREVIATIONS

ALD	Atomic Layer Deposition
at. %	Atomic percent
CBD	Chemical Bath Deposition
CPV	Cyclic Photo Voltammetry
CuO	Copper (II) Oxide
Cu_2O	Cupper (I) Oxide.
CVD	Chemical Vapor Deposition
DC	Direct Current
E-H	Electron – Hole
FETs	Field Effect Transistors
FF	Fill Factor
HEP	Hydro-Electric Power
I-V	Current versus Voltage
LED	Light Emitting Diode
NWs	Nanowires
OJL	O'Leary, Johnson, Lim

PDT	Post Deposition Treatment
PEC	Photo Electrochemical
PMT	Photomultiplier
P- V	Power versus Voltage
PVD	Physical Vapor Deposition
SEM	Scanning Electron Microscopy
XRD	X-Ray Diffraction
ZnS:Al	Aluminium doped Zinc Sulfide
η	Conversion efficiency
ρ_s	Sheet resistivity
α	Absorption coefficient

ABSTRACT

Semiconductor materials have been used in fabrication of a variety of electronic devices for example solar cells, photo-detectors, integrated circuits (ICs), light emitting diodes (LED) among others. A lot of focus is on thin film solar cell due to the rising need for low cost and renewable sources of energy. A variety of semiconductor materials like Ge, Si, Al, GaAs, $CuInSe_2$, have been employed in fabrication of thin film solar cells. Cu_2O and aluminum doped ZnS thin films are promising materials for the development of future generation low cost and higher efficiency thin film solar cells. Cu_2O thin film has a low band gap and high absorption co-efficient while ZnS:Al has good optical transmission in the visible spectral range. However, very little data in literature is available on Cu_2O-ZnS:Al p-n junction. Therefore in this work, Cu_2O and ZnS:Al thin films were coated on glass slide by DC reactive sputtering and evaporation methods, respectively using Edward Auto 306 evaporation system. Cu_2O- ZnS:Al p-n junction was fabricated by DC reactive sputtering evaporation methods on a glass substrate. Transmittance and reflectance of both Cu_2O and ZnS:Al thin films were measured using Spectrophotometer 3700. Absorption of the thin films was calculated from the transmittance and reflectance data. The transmittance data was analyzed by scout software models to obtain band gap. Transmission of Cu_2O films decreased from 43% to about 30% for films with thicknesses 50 nm to 250 nm. All the films showed high absorption of above 50% within the visible region. Absorption of Cu_2O films increased with thickness, with highest absorption of about 60% for thin films of thickness 200 nm. For ZnS:Al, transmission increased from 68% for undoped ZnS to 85% for Al dopant concentration of 6 at% dopant concentration. The band gap of Cu_2O decreased from 2.452 eV to 2.402 eV for film thicknesses range 50 nm to 250 nm. Electrical properties of Cu_2O and ZnS:Al thin films, at room temperature were measured using four point probe method whereby measurements were made using Keithley 2400. The electrical resistivity of ZnS:Al thin films decreased from 1.54×10^5 Ωcm for undoped ZnS thin film to 69 Ωcm for Al concentration of 6 % dopant concentration. Resistivity of Cu_2O films increased from 7 Ωcm to 53 Ωcm with increase in thicknesses from 50 nm to 250nm. The I-V measurements were obtained using Solar Simulator. From I-V characteristics of Cu_2O- ZnS:Al p-n junction, fill factor (FF) was found to be 0.629, conversion efficiency (ŋ) was 0.62%, Short-circuit current (I_{sc}) was 1.0×10^{-2}A and open circuit voltage (V_{oc}) was 0.592V. ZnS:Al and Cu_2O thin films are therefore suitable for making solar cells. In addition to optical and electrical characterization of Cu_2O and ZnS:Al thin films, studies on the morphology of the glass used for the slides and its effects on the efficiency of the solar cell also need to be done

CHAPTER ONE

INTRODUCTION

1.1 Background to the study

The global main energy sources are non-renewable, but these sources have been faced with high demand, thus may possibly be depleted in the near future. Apart from being non-renewable, fossil fuels, especially petroleum and coal have greatly contributed to the rising problem of global warming and pollution. The soaring problems of pollution by the emitted gases and possible depletion of these energy sources have prompted the international community to shift their focus to renewable energy, with solar energy being the likely main alternative (Balzani *et al.,* 2010). The primary source of light energy is the sun; a resource that is transferred directly from the sun through space in the form of electromagnetic radiations within the wavelengths ultra-violet to infra-red and radio waves i.e 0.2 μm to 3 μm. This energy has been provided steadily with a life time projection of over 10 billion years, constant irradiative energy output (Sze, 1981).

Conversion of light energy directly to electrical energy by application of the electronic properties of semiconductors is a pleasingly innovative and simple energy transformation process, and an effective alternative to ordinary energy sources. Some outstanding uses of solar cells over the last 50 years are: supply of electrical energy in remote areas, weather forecasting, lighting, communication and water pumping systems used in developing countries; supply of electrical energy for consumer products such as electronic calculators and domestic lights; and for use in space, for example in space vehicles and satellites (Robert *et al.*, 2007).

Oxides of metals have shown a variety of useful properties based on their crystal structure as well as the bonds between the metal cation and oxygen (Rakhshani, 1986). The electrical properties of metal oxides range from insulating to highly conducting like metals, or even superconducting. Because of this diverse functionality, metal oxides have become the most fascinating inorganic materials in device applications, for example; LEDs, field effect transistors and solar cells. Among the metal oxides, Cu_2O is attractive because Cu metal is abundant on earth, has low processing cost and is non-toxic. Moreover, this oxide has desirable optical and electrical properties such as low band gap and high absorption of light, which may find use in a wide range of electrical devices (Kylner, 1999; Ohtomo *et al.,* 2005).

1.2 Statement of the Research Problem

Besides the possible depletion of fossil energy resources for instance gas, coal and oil, they have contributed to unreliable climate changes through emission of high levels of greenhouse gases (for example Carbon(IV)Oxide, carbon monoxide, sulphur dioxide) and acidification (Balzani *et al.,* 2010). On the other hand, traditional silicon cells manufacturers are currently facing new challenges due to the high processing cost, weight and fragility of silicon. Therefore there is need for alternate, low cost, reliable and environment friendly source of energy.

1.3 Objectives

1.3.1 General Objective

To investigate the optical and electrical properties of Cu_2O and Al doped ZnS thin films for solar cell applications.

1.3.2 Specific Objectives

i. To deposit different samples of ZnS:Al thin films by evaporation
ii. To deposit Cu_2O thin films on glass substrate by DC reactive sputtering
iii. To study the optical and electrical properties of Cu_2O and ZnS:Al thin films
iv. To Fabricate a Cu_2O-ZnS:Al p-n junction
v. To determine the I-V characteristics of Cu_2O-ZnS:Al solar cell at room temperature and obtain the solar cell parameters from the I - V characteristics.

1.4 Rationale

Demand for electrical energy has greatly risen, resulting in a crisis of availability of a clean and reliable energy. This energy crisis is due to natural degradation of environment, unreliability and possible strain on other sources of energy such as hydro-electric power, fossil fuels and nuclear energy among others. Consequently, this has prompted research in solar cell applications as a reliable alternative source of electrical energy (Balzani *et al.*, 2010). Solar cell technology has gone through immense expansion over the last forty years, initially for provision of electrical energy for space crafts and currently for terrestrial applications.

Recently, there have been enormous investments on processing facilities which are majorly for silicon-based technologies, with over a 93% market share, mainly due to its maturity and huge government subsidies in the world's greatest users of solar energy such as Germany (Green, 2004). However, there is currently emerging challenges on silicon due to new wave of thin-film technologies. Manufacturers of silicon solar cells are currently limited by the high processing cost, weight and fragility of silicon. Thin film solar cells, using Cu_2O-ZnS: Al p-n junction is a reliable alternative since the production process of Cu_2O is simple, it is nontoxic and the starting material (copper) is abundant (Papadimitropoulos *et al.*, 2005).

CHAPTER TWO

LITERATURE REVIEW

2.1 Copper (I) Oxide

Sharma, (1979) investigated the properties of Cu_2O and reported that it is a nontoxic material, suitable for use in electronic devices as well as oxygen and humidity sensors. The optical properties studied on copper(I)Oxide semiconductors showed high optical absorption (Olsen *et al.* 1979; Herion *et al.*, 1980).

Rai (1988) investigated optical properties of Copper (I) oxide. The results showed that Cu_2O had a direct band gap of 2.0 eV, suitable as an absorber layer in heterojunction solar cells.

Studies on $CuAlO_2$ and $SrCu_2O_2$, which are Cu_2O related materials, reported transparent conducting oxides with p-type conductivity. Although $CuAlO_2$ and $SrCu_2O_2$ had identical electronic structure to Cu_2O, they had wide band gaps. The p-type conductivity of Cu_2O could be attributed to the existence of Cu vacancies, which form acceptor levels above the valence band. The deposition method and parameters greatly influenced the physical properties of the films (Robertson *et al.*, 2002).

Kobayashi *et al*. (2007) investigated the optical properties of Cu_2O thin films prepared by halide chemical vapor deposition on MgO (110) substrate under atmospheric pressure. CuI was evaporated from a boat at a temperature of 883 K with O_2 as the reactive gas and N_2 carrier gas. The calculated value of optical band gap energy of Cu_2O thin film was

2.38 eV. High-quality Cu_2O films were obtained from the reaction of CuI and O_2 in atmospheric pressure.

Ogwu *et al.* (2005) investigated the effects of argon–oxygen flow rates on optical properties of Copper(I)Oxide thin films coated on glass slides by reactive radio frequency magnetron sputtering. Optical transmission in the films was measured in the spectral range 400 nm to 850 nm. The thin films showed optical transmission range of 40% to 80% for Copper(I)Oxide films deposited at a low rf power of 200 W, for different oxygen flow rates. The optical band gap values of the films were in the range 2.05 and 2.4 eV.

Mugwang'a *et al.* (2012) studied the optical properties of Copper Oxide thin films prepared by reactive DC magnetron sputtering. The thin films had low reflectance of below 45% and high absorption. The Tauc curves showed direct transition with band gaps ranging between 1.62 eV to 2.54eV for oxygen flow rates of 5 sccm to 22.5 sccm.

Pan *et al.* (2016) investigated the effects of temperature and oxygen flow rate on CuO and Cu_2O thin films prepared by DC reactive sputtering. Their results showed that Cu_2O thin films had a critical absorption edge in the spectral range around 400 nm. They also had good absorption within the spectral range of 400 nm to 570 nm and a very strong absorption edge appearing at a wavelength of around 570 nm. CuO thin films had high absorption at wavelengths in the NIR range. These results suggest that Cu_2O thin films are candidates for solar-cell devices and CuO thin film is a candidate for near-IR detectors.

2.2 Zinc Sulfide

ZnS thin films have been prepared by thermal evaporation and the effect of their thicknesses on the optical properties of photovoltaic p-n junction (silicon photocell) investigated. Optical band gap of the films were in the range 3.2 eV to 3.3 eV for thicknesses 100 nm to 300 nm. Electrical studies revealed that the thin film exhibit n–type conductivity and the hall coefficient decreased with increased thickness. The films used had polycrystalline structure (Kushkul, 2001).

Jiang *et al*. (2012) investigated the influence of aluminium doping in simple co-evaporation in ZnS nanowires. Results showed great improvement in the conductivity of ZnS by a wide magnitude by adjusting the doping level. Field effect transistors (FETs) fabricated from individual ZnS:Al nanowires (NW), revealed charge carrier concentration of approximately 1.3 x $10^{-18}$$cm^{-3}$ in the NWs.

2.3 Copper Based Solar Cells

Papadimitriou *et al*. (1981) fabricated ZnO/Cu_2O and CdS/Cu_2O junction solar cells. For ZnO/Cu_2O, the highest open – circuit voltage (V_{oc}) was 0.3 V. It was noted the cell characteristics were dictated by a copper rich region formed adjacent to Cu_2O substrate. For the case of CdS/Cu_2O, heterojunction formed at room temperature the I_{SC} and V_{oc} were 2 $mAcm^{-2}$ and 0.4 V, respectively. The films used on the solar cells had a transmittance of approximately 70 % upto 1.5 eV energy radiations. The sheet resistance of the films with a thickness of 22 nm was 70 Ω/cm^2 (when evaporated on glass).

Hetero-junction solar cells with p-Cu_2O and n-ZnO fabricated by electro-deposition and photochemical deposition methods have been reported (Izaki *et al.*, 2006). The fabricated cells had an efficiency of approximately 2%.

In this work the optical and electrical properties of both Cu_2O and ZnS: Al thin films were investigated for their suitability for solar cell applications.

CHAPTER THREE

THEORETICAL CONSIDERATIONS

3.1 Semiconductor Materials

Semiconductor materials have their electrical conductivities lying between that of conductors such as copper, gold and other metals and insulators, such as glass. When the temperature of semiconductors is increased their resistance decreases, unlike metals whose resistance increases with temperature (Sze, 2008). Their conductivity may be improved by doping. Doping is the introduction of small amounts of impurities into the crystal structure of an intrinsic semiconductor. Doping leads to creation of two types of materials i.e. p-type or n-type semiconductors. A semiconductor junction is created between any two differently-doped layers within the same crystal (Pankove, 1975).

A p-n junction made from semiconductor materials exhibit a variety of desirable characteristics for example infinitely high resistance to flow of current in one direction and very low resistance to current flow in the other direction, variation in resistance at different temperatures and sensitivity to light or heat. Semiconductor devices find applications in amplification, switching and energy transformation since their electrical properties can be adjusted by doping (addition of small amounts of impurity), application of electric fields or light (Pankove, 1975).

3.1.1 Intrinsic Semiconductor

This is an extremely pure semiconductor material. The conduction in an intrinsic semiconductor takes place when electrons from the top of the valence band are thermally

excited to the bottom of the conduction band. The Fermi level E_F for a pure semiconductor lies at the middle of the energy gap. The probability of finding an electron within the forbidden gap is 0.5 eV (Serhan, 2005).

3.1.2 Extrinsic Semiconductor

This is a semiconductor material whose conductivity has been altered by doping. Doping refers to the addition of controlled amounts of impurity to an intrinsic semiconductor. Doping leads to introduction of extra holes or electrons within the crystal. An extrinsic semiconductor with extra free electrons is known as "n-type" while that with extra holes is called "p-type". The semiconductor materials used in electronic devices are doped at high precision to regulate the amount and regions of p-type and n-type dopants. Many p and n regions can be created within a single semiconductor crystal leading to formation of multi-junctions within a crystal. These multi-junctions can be responsible for the desirable electronic behavior (Kittel, 1995).

3.2 Thin Film Solar Cell

A Solar cell is basically a p-n junction capable of converting light energy directly into electricity by photovoltaic effect (Markvat, 1998). When light energy falls on a p-n junction, photons with excess energy *(hv*) over the band gap of the material are absorbed creating electron-hole (E-H) pairs which are the charge carriers; a photocurrent is thus generated (Wielder, 1982). The internal junction electric field leads to separation of the created electron-hole pairs. Holes drift to one electrode and electrons are repelled to the n region and finally leave through the external contact (Stone, 1993) as in figure 3.1

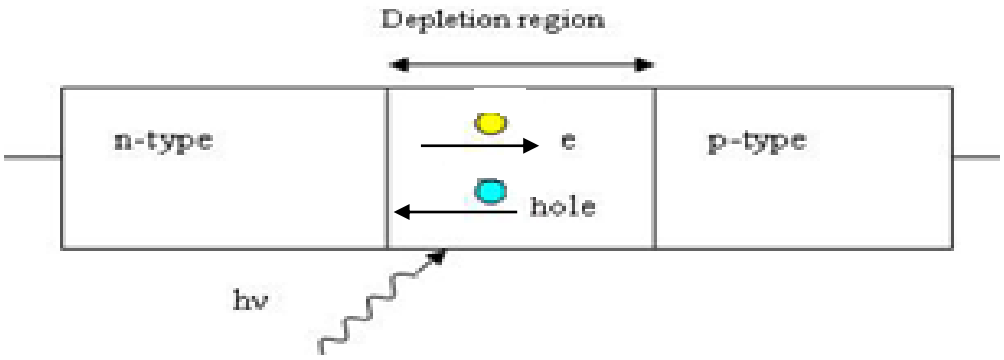

Fig. 3.1: Diagram of p-n heterojunction solar cell (Würfel et al., 2015)

The electron-hole pairs increase the concentration of minority charge carriers. The decrease in potential energy barrier allows current to flow easily across the junction and a voltage V_{oc} is developed between the junction (Tsubomura *et al.*, 1993; Stone, 1993). The value of V_{oc} developed across the junction depends on the band gap energy of the absorber material. Equation 3.1 can be used to calculate maximum V_{oc} (Kemell, 2003), where e is electron charge and E_g is band gap of the material.

$$\boldsymbol{Max.V_{oc}} = \frac{E_g}{e} \qquad (3.1)$$

Band diagrams of p-n junctions are shown in figures 3.2 and 3.3

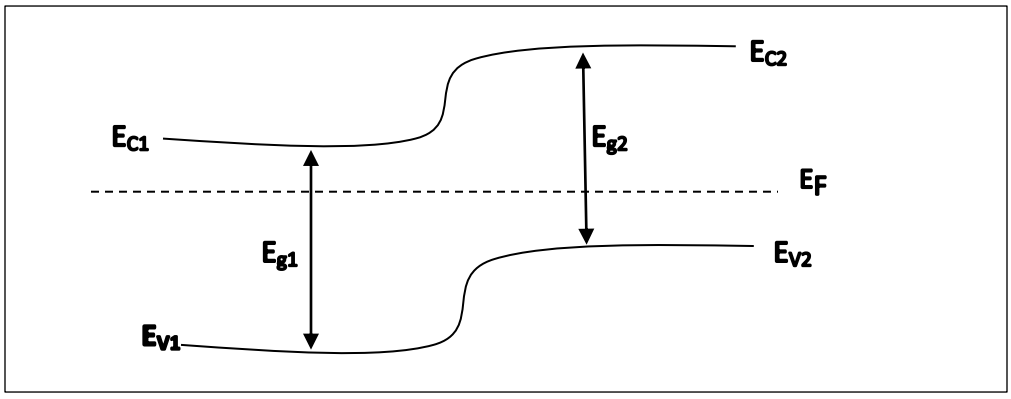

Fig. 3.2: P-N heterojunction at thermal equilibrium in dark (Würfel *et al.*, 2015)

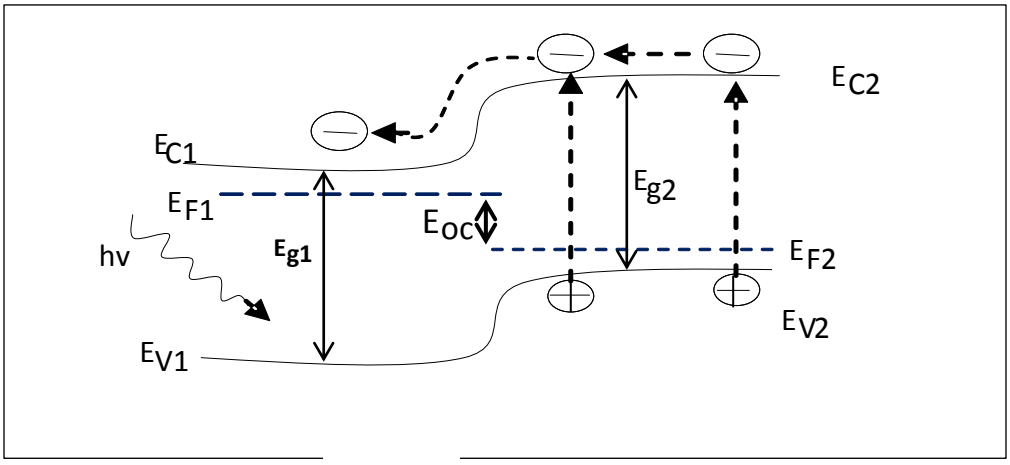

Fig. 3.3: P-N heterojunction under illumination in open circuit, where 1 and 2 are n-type and p-type materials, respectively (Würfel *et al*., 2015)

3.2.1 Equivalent Circuit of Solar Cell

A perfect solar cell may be modeled by a current source in parallel with a diode. However the efficiency of a practical solar cell is reduced during operation by power loss due to the internal resistances. These internal resistances can be represented as parallel shunt, and series resistances, R_{SH} and $R_{S,}$ respectively. Figure 3.4 shows schematic diagram for an equivalent circuit for a solar cell (Eduardo, 1994).

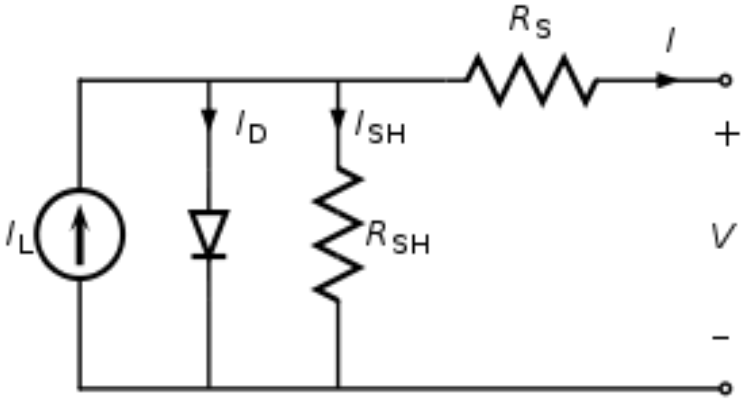

Fig. 3.4: Equivalent circuit of photovoltaic cell (Eduardo, 1994)

3.3 Thin Film Preparation

Thin film deposition methods are grouped into two major classes namely Physical Vapor Deposition (PVD) and Chemical Vapor Deposition (CVD). Examples of PVD method are sputtering technique and thermal evaporation technique. Examples of CVD methods are molecular beam epitaxy, liquid vapor deposition and metal oxide chemical vapor Deposition (Ohring, 1992). In this research, copper(I)oxide thin film was deposited by sputtering while ZnS:Al thin film was deposited by evaporation technique.

3.3.1 Evaporation Method

Evaporation is a physical vapour deposition method in which atoms are vaporized from a boat by application of heat. The evaporation chamber is always pumped to very low pressure of about 10^{-5}mbars (Ohring, 1992). The evaporation chamber is normally highly evacuated to minimize contamination. The starting material is placed on a boat at high temperature and vaporized or sublimed. The gaseous atoms or molecules then condense on the substrate. The deposited atoms or molecules eventually re-arrange on the substrate's surface with modified bonding.

The boat containing the evaporant is a highly resistive material between the anode and cathode to allow the passage of high direct current. Boats made from molybdenum or tungsten are usually used in deposition of low melting point compounds. Figure 3.5 is a schematic diagram of evaporation system;

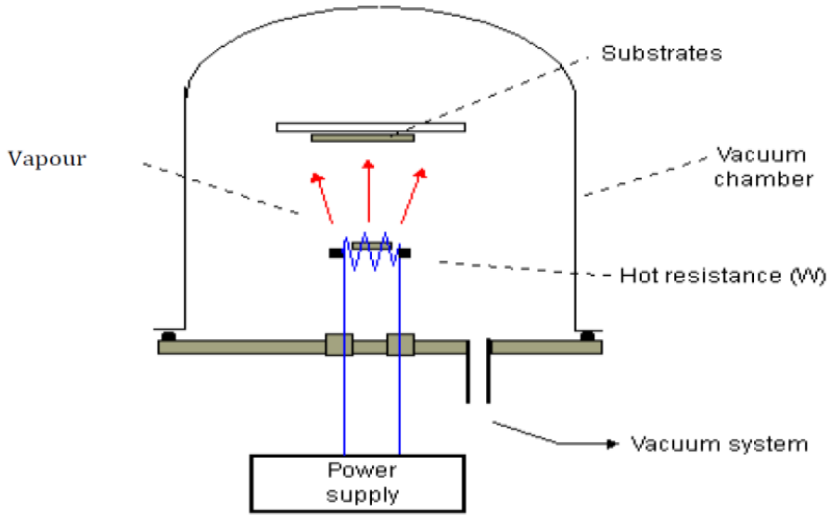

Fig. 3.5: Typical thermal evaporation system showing the various components involved in the process

For the vaporization of high melting point, compound sample is normally bombarded by highly energetic electrons from an electron gun within the chamber. Compound films can be obtained by evaporation from two or more boats (Gunther, 1966). The rate of evaporation of the sample is mainly affected by temperature.

3.3.2 Sputtering Method

Sputtering is a physical vapour deposition technique in which atoms are ejected by bombardment of the surface of a material with energetic particles (Ohring, 1995). The bombarding particles may be ions emerging from plasma at low pressure, ejecting atoms or molecules which are subsequently deposited on a substrate. The displaced lattice atoms and the bombarding particles collide with surface atoms, ejecting them leading to a chain reaction of collisions as shown in figure 3.6.

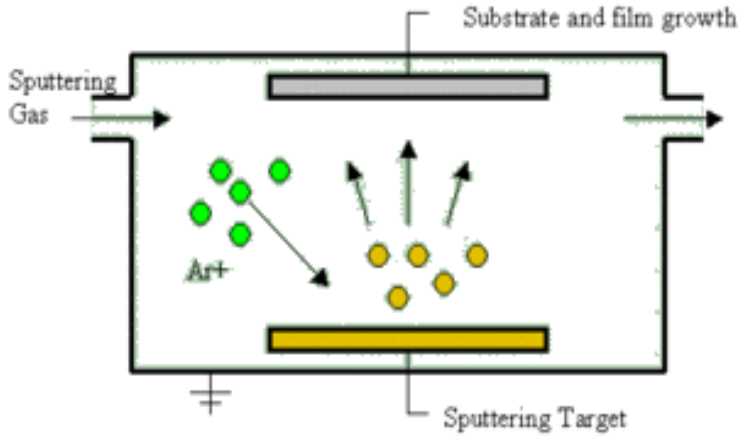

Fig. 3.6: Schematic presentation of a typical sputtering system (Matsunanmi *et al*., 1980)

Direct current sputtering is mainly used for metal targets, or targets made of materials that are electrically conducting so that they can act as an electrode. Direct current sputtering is achieved by connecting the surface of a target to a high negative potential, thus attracting positive ions from the plasma. When the sputtering chamber is operated at a very low pressure, a high potential across the electrodes, and a high series resistance of about 10 kΩ, the ions are attracted to the negative electrode and bombard the target to dislodge the surface atoms. The dislodged atoms move through the medium and condense on the substrate. Both conductors and insulators can be used for a target. A radio frequency field (of about 13 MHz) may also be applied to the target, whereby a capacitor is connected in series with metallic target so that it is coupled with the RF voltage. Alternatively, an insulating surface is usually bonded to a metal backing electrode to create a capacitive component (Maissel, 1966).

The sputtering chamber is normally pumped to a low pressure of below 10^{-6} torr and the argon is allowed in at a pressure of 20 mtorr. When RF voltage is applied, a plasma is struck where positive ions are attracted to the target during each negative half cycle. The attraction of more ions leads to a build-up of a negative bias due to higher movement of

electrons than that of ions in the plasma. The subsequent half cycle of the RF fields then accelerates the ejected atoms from the target to the substrate. The substrate is kept at relatively low temperature to ensure that crystallization is inhibited; thus the deposited species forms an amorphous film at sufficiently low mobility of atoms. This method can produce homogeneous and uniformly thick samples (Maissel, 1966).

Sputtering using RF field has advantage over evaporation method since it can be used to produce compound films because the targets are already in compound form. This is because of limited variation in sputtering rates for different elements, unlike melting points of different elements, vapour pressures which affect evaporation rates. In sputtering, the stoichiometry of the starting materials tends to be maintained in the resulting films (Oladeji *et al.*, 2005).

Reactive sputtering involves the use of reactive gases for example oxygen or nitrogen gas, which chemically react within the chamber. Reactive sputtering increases the sputtering rate and helps in incorporation of desired atoms into the films. An example of reactive sputtered film doped amorphous silicon films is Ar : H_2 : N_2 /PH_3 mixture (Meinel *et al*., 1976).

Various factors for example the ratio of partial pressure of reactive sputtering, RF power applied to target, sputtering pressure and bias voltage of target or substrate may cause variations in structural, optical and electrical properties of the films produced by sputtering process (Ohring, 1995).

3.4 Thin Film Characterization

The properties of thin films that can be investigated include optical, electrical and structural properties. In this work optical and electrical properties of the thin films were investigated.

3.4.1 Optical Characterization

The optical properties of thin films for example transmittance and reflectance can be measured directly while absorbance can be calculated from the transmittance and reflectance data, using equation 3.2.

3.4.1.1 Transmittance and Reflectance

Reflectance and transmittance are investigated by use of optical spectrum analyzer. Optical measurements are carried out using spectrophotometer machine in the spectral range from 200 nm to 1400 nm. Figure 3.7 shows how optical transmission measurements are obtained.

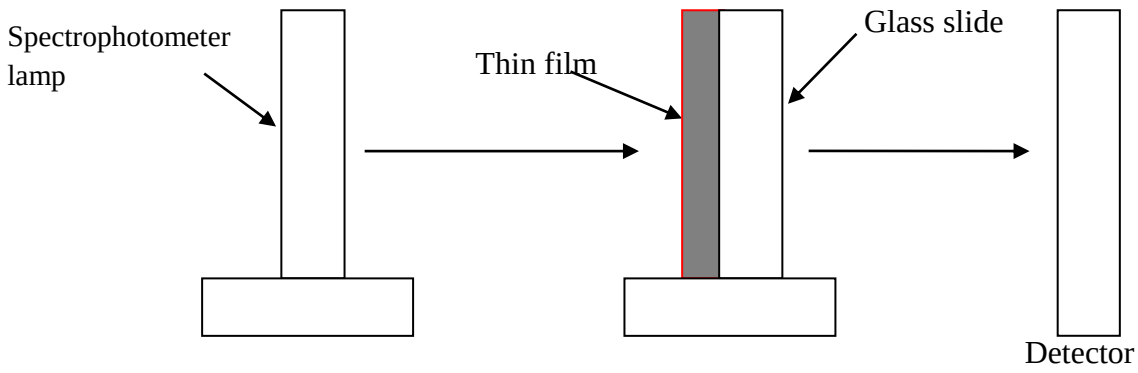

Fig. 3.7: Schematic diagram for optical measurements

An accurate measurement of the band gap is achieved by directing light of known intensity, I_o and wavelength on a film of thickness *l* and the relative transmissions of the light measured. Photons with excess energies over the band gap (E_g) are absorbed while those of lower energy are transmitted. Transmittance and reflectance data are directly measured by the spectrometer while absorbance is calculated from the transmittance and reflectance data using equation 3.2. Optical absorption of a given film depends on optical band gap of the film, thickness of film and photon wavelength (Pankove, 1975)

$$A + T + R = 1 \tag{3.2}$$

The transmittance of a thin film is the ratio of intensity of the transmitted photon, I_t to the intensity of the incident photon, I_o. Transmittance can be calculated using equation 3.3 (Lothian, 1958);

$$\text{Transmittance (T)} = \frac{I_t}{I_o} \tag{3.3}$$

For an incident monochromatic beam of light of known frequency and intensity, much of the beam is absorbed and a small fraction of incident light is transmitted. Intensity of the reflected light, I_R, is measured by a detector. Reflectance is given by the equation 3.4;

$$\text{Reflectance (R)} = \frac{I_R}{I_o} \tag{3.4}$$

The transmittance and reflectance data can be analyzed using scout software to obtain optical constants such as band gap and absorption coefficient.

3.4.1.2 Absorbance

When radiation of intensity I_o is incident on a material of thickness *l*, the transmitted intensity I_t is given by equation 3.5;

$$I_t = I_o \exp(-\alpha l) \tag{3.5}$$

where α is the absorption coefficient, given by equation 3.6;

$$\alpha = \frac{1}{l} \ln\left[\frac{I_o}{I_t}\right] \tag{3.6}$$

3.4.1.3 Optical Band Gap

The energy required to move a valence electron into the conduction band is called the band gap (E_g). From Tauc's relation, the absorption coefficient depends on the energy of photon and is given by equation 3.7;

$$\propto = \frac{(h\boldsymbol{\nu} - E_g)^n}{h\boldsymbol{\nu}} \tag{3.7}$$

where *h* is the Planck's constant, $\boldsymbol{\nu}$ is frequency of the radiation and *n* is the type of transition. The transition of electron from valence band to conduction band may be direct or indirect; $n = \mathbf{\frac{1}{2}}$ for direct transition (Mehta *et al*., 2010). Equation 3.7 therefore leads to equation 3.8, on substitution for n and rearranging;

$$(\propto h\nu)^2 = h\nu - E_g \tag{3.8}$$

When a graph of $(\propto hv)^2$ against hv is plotted, a curve with a linear portion is obtained. The band gap, E_g is obtained by extrapolating the straight part of the curve onto the energy axis i.e $(\propto hv)^2 = 0$.

3.4.2 Scouts Software

Scouts software consists of several models namely OJL, Harmonic Oscillator, Dude, Tauc Laurent models and many more.

3.4.2.1 OJL Model

OJL model describes inter band transitions in non-crystalline materials. It is used to determine the density of states for optical changes into the conduction band from the valence band. In this model the assumption made is that parabolic bands have tail states that exponentially decay into the band gap as shown in figure 3.8.

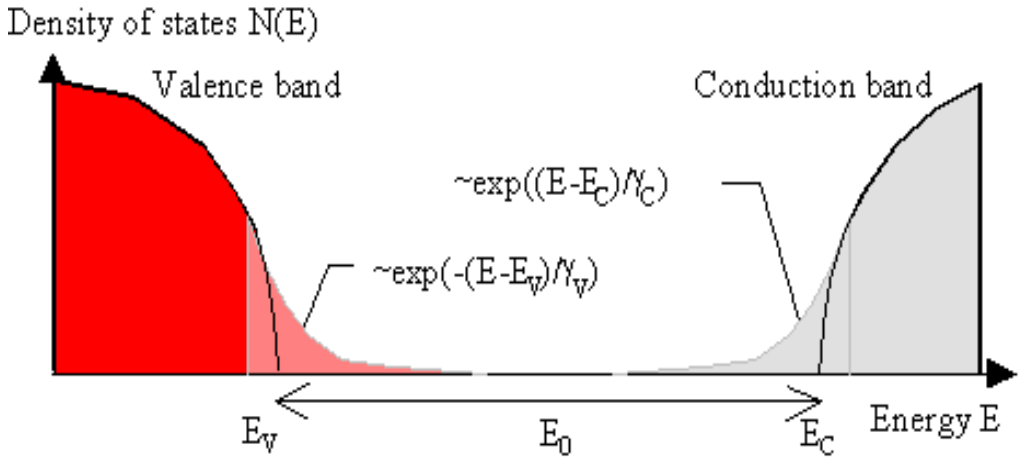

Fig. 3.8: Graph of Density of States against Energy for OJL model (O'Leary *et al.*, 1997)

The mobility edges of the valence and conduction band are given by equations 3.9 and 3.10, respectively;

$$E_{m,V} = E_V - \frac{1}{2}\gamma_V \quad (3.9)$$

and

$$E_{m,C} = E_C + \frac{1}{2}\gamma_C \quad (3.10)$$

where E_V and E_C are energies at the top valence and bottom conduction bands respectively, γ_V and γ_C, the damping constants with corresponding masses m_V and m_C.

The mobility gap, E_o in the OJL model is therefore given by equation 3.11;

$$E_o = E_C + \frac{1}{2}\gamma_C - (E_V - \frac{1}{2}\gamma_V). \quad (3.11)$$

The band gap is obtained by getting the difference between E_V and E_C values, assuming there's no disorder, that is both γ_V and γ_C are zero.

3.4.2.2 Drude Model

In the case of doped semiconductors the charge carriers set free by the donors or acceptors can be accelerated by very little energies and hence do respond to applied electric fields with frequencies in the infrared region. Drude model gives an expression for the susceptibility of free carriers (which is also applicable to metals) as well as concentration and damping constants.

$$\chi_{Drude}(\nu) = \frac{\Omega_P^2}{\nu^2 + i\nu\Omega_\tau}, \quad \text{with } \Omega_P^2 = \frac{ne^2}{\varepsilon_0 m} \quad (3.12)$$

where Ω_P is plasma frequency, Ω_τ damping constant, n is charge carrier density, m is effective mass and e is elementary charge.

3.4.2.3 Harmonic Oscillator Model

This model is used in material identification. Microscopic vibrations involving motion of heavier atomic nuclei than electrons have their resonance frequencies in the infrared region. In the case of silicon important impurities like carbon and oxygen are detected by their characteristic vibrational modes. These characteristic frequencies depend on the oscillating masses and the strength of the bonds as given in equation 3.13.

$$\chi_{Harmonic} = \frac{\Omega_P^2}{\Omega_{\mathrm{TO}}^2 - v^2 - iv\Omega_\tau} \tag{3.13}$$

where Ω_P is oscillator strength, Ω_τ doping and Ω_{TO}resonance position.

3.4.3 Electrical Characterization

Electrical characterization can be done using Four point probe method.

3.4.3.1 Four Point Probe Method

This method can be used to find the resistivity of semiconductors, both of bulk and thin film samples. It can also be used to determine whether a material is causing insulation on a conducting substrate. Current is drawn from a power source (DC) with a high internal resistance through the two outer contacts and the voltage between the two inner contacts measured using a voltmeter with a high internal resistance. Figure 3.9 shows an arrangement for electrical measurements.

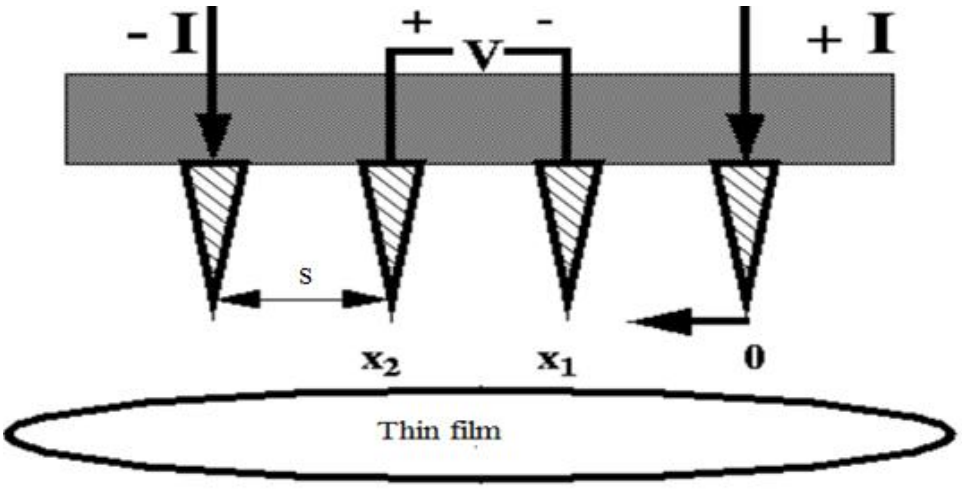

Fig. 3.9: Schematic diagram of four point probe set-up, where s is the distance between the probes (Chan, 1994).

The probes are connected to Keithley 2400 Source Meter. Current is sourced though the outer electrodes while voltage readings are taken between the inner electrodes. Sheet resistance is described by equation 3.14;

$$\Delta R = \rho \frac{dx}{A} \tag{3.14}$$

where ρ is the resistivity and A is the active area of the solar cell. For a very thin film, the film thickness, *t*, is much smaller than *s* (the probe separation distance) and current rings are formed through the sample. The area can therefore be given by equation 3.15;

$$A = 2\pi xt \tag{3.15}$$

Taking the integral over the inner probes, leads to equation 3.16;

$$R_s = \int_s^{2s} \frac{\rho}{2\pi xt} \frac{dx}{x} = \frac{\rho}{2\pi t} \ln(x) \Big|_s^{2s} = \frac{\rho}{2\pi t} \ln 2 \tag{3.16}$$

Hence;

$$\rho = \frac{2\pi tR}{\ln 2} \qquad (3.17)$$

3.5 I-V Characteristics of Thin Film Solar Cells

Solar cell characterization is done using a solar simulator. Figure 3.10 shows a schematic diagram for I-V measurements.

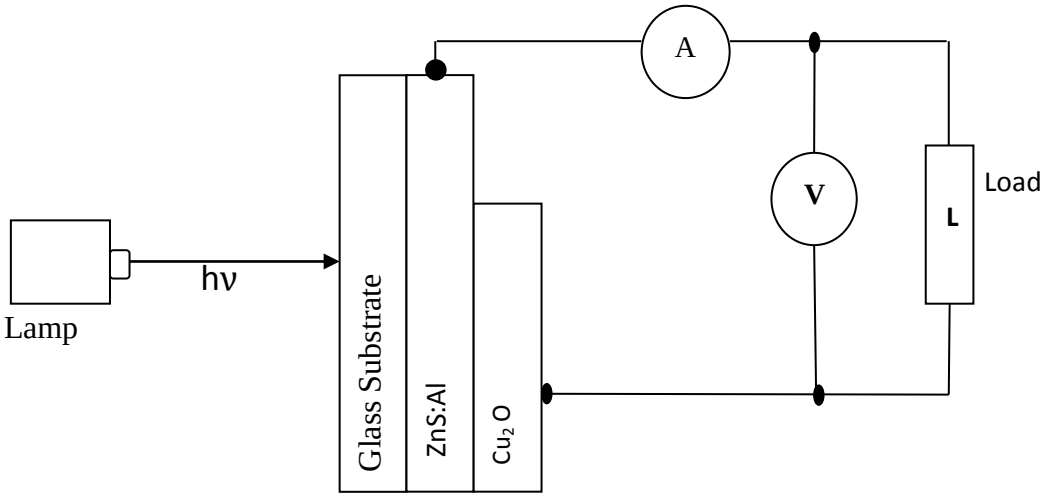

Fig. 3.10: Schematic diagram for measurement of I-V characteristics

An I-V curve of a solar cell is the superposition of the I-V curve in the dark with the light generated current. When a p-n junction is illuminated, the I-V curve shifts down into the fourth quadrant as shown in figure 3.11, where power can be extracted from the diode.

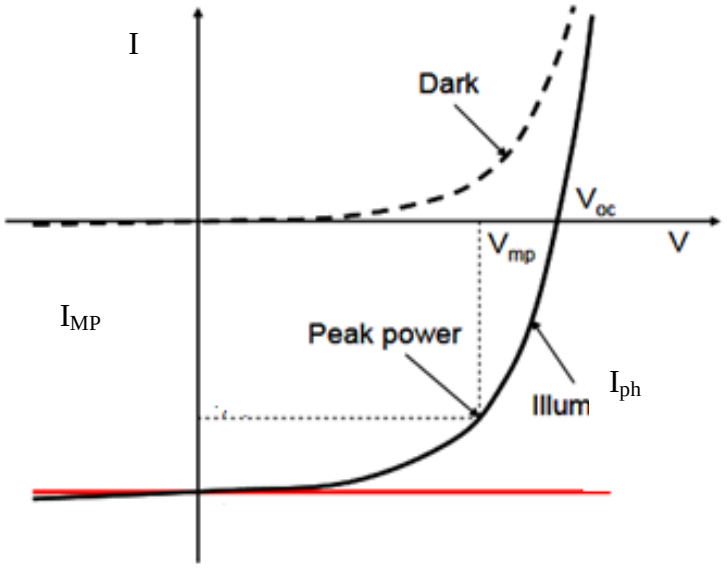

Fig. 3.11: Typical I-V Characteristics of a p-n junction in the dark and under illumination (Green, 1982)

The current diverted by the diode is given by Shockley equation 3.18;

$$I = I_o \left\{ \exp\left(\frac{V_j}{nV_T}\right) - 1 \right\} \tag{3.18}$$

where, I_o is reverse saturation current, $V_T = \frac{kT}{q}$; q is electron charge, n is diode ideality factor, k is Boltzmann's constant and T is absolute temperature

The main external parameters used to characterize solar cells include Short- circuit current, open circuit voltage, fill factor and energy conversion efficiency.

3.5.1 Short-Circuit Current, I_{SC}

This is the current that flows through the external circuit when the electrodes of the solar cell are short- circuited. Ideally, Isc equals to the photo-generated current density Iph. The largest current is always achieved under short circuit conditions as in equation 3.19;

$$\mathrm{I(at\,V = 0) = I_{sc} = I_L} \tag{3.19}$$

3.5.2 Open-Circuit Voltage, V_{OC}

This is the potential difference across the output terminals of a solar cell at open circuit conditions i.e when I = 0. The open-circuit voltage is equal to the amount of forward bias on the solar cell due to the bias of the solar cell junction with the photo-generated current. The open-circuit voltage depends on the photo-generated current density and it is given by equation 3.20 (Sze, 1981; Markvart, 1998).

$$V_{oc} = \frac{AkT}{q} \ln\left[\frac{I_L}{I_o} + 1\right] \tag{3.20}$$

3.5.3 Fill Factor, FF

Fill factor is a measure of quality of a solar cell. It is the ratio of the maximum power (Pm = Imp × Vmp) deliverable by a solar cell to the product of Voc and Isc. Fill factor can be calculated from equation 3.21;

$$\mathrm{FF} = \frac{\mathrm{V_{max} I_{max}}}{\mathrm{V_{oc} I_{sc}}} \tag{3.21}$$

3.5.4 Efficiency, ŋ

With the power input due to the incident light (P_{in}) on p-n junction, the efficiency of the solar cell is the ratio of maximum power output to power input as shown in equation 3.22 (Pethe, 2003).

$$ŋ = \frac{P_{max}}{P_{in}} \tag{3.22}$$

But $P_{max} = I_{SC}V_{OC}FF$

Therefore,

$$ŋ = \frac{\boldsymbol{I_{SC}V_{OC}FF}}{P_{in}} \tag{3.23}$$

CHAPTER FOUR

MATERIALS AND METHODS

4.1 Deposition of Cu_2O and ZnS: Al Thin Films

4.1.1 Substrates Cleaning

The glass slides to be used as substrates for deposition of the thin films were washed successively with acetone, alcohol and distilled water then heated in an oven at 120 ^{0}C to remove any moisture or methanol present.

4.1.2 Cu_2O Thin Films

Cu_2O thin films were coated on glass substrates by DC reactive magnetron sputtering. The target substrate distance was 13cm. The sputter chamber was evacuated to a low pressure of 5 x10^{-4} mbars. Copper target of high purity was powered by advanced energy 200W power generator. The substrate temperature was maintained at 300 K. Sputtering gas used was argon while oxygen gas was used as the reactive gas. The flow of oxygen and argon gases from needle valves into the sputter chamber was regulated by Tylan mass flow controllers (Model FC-260). The substrate was covered with a shutter and copper target was pre-sputtered in pure argon atmosphere for 15 seconds, to ensure that the sputter target was free from any oxide that might have formed on the surface. The sputter chamber was pumped down again to 5 x10^{-4} mbars, and sputtering done with oxygen partial pressure of 2 x10^{-2} mbars. Argon gas was introduced into the chamber to maintain the required total sputter pressure. The sputter duration for the five samples was varied from 10 to 50 seconds in order to produce thin film samples of different

thicknesses. The flow of argon gas was stopped first after deposition of the thin film. Table 4.1 shows a summary of deposition conditions during preparation of Cu_2O films.

Table 4.1: Summary of deposition parameters for Cu_2O thin films

PARAMETER	VALUE
Sputtering target	copper (99.99% pure)
Target-substrate distance	13cm
Base pressure	5×10^{-4} mbars
Oxygen partial pressure	2×10^{-2} mbars
Substrate temperature	300K
Sputter time	10 – 50 Seconds
Cathode current	200 mA

4.1.3 Preparation of ZnS:Al Alloys

Six samples of ZnS: Al alloys were prepared using highly pure (99.999 %) elemental zinc and sulfur granules using predetermined mass ratios. Each sample of zinc and sulfur granules was weighed and placed in a clean silica glass tube. Six different proportions of aluminium (i.e 0%, 2%, 4%, 6%, 8% and 10%) were weighed and each added to the ZnS samples which were then purged with argon to expel and exclude air. The alloy samples were then heated to about $700\ ^0$ C using oxyacetylene burner and then allowed to cool. Reheating and cooling was repeated three times while shaking the sealed tube to ensure

homogeneity of the samples. The samples were then ground in a porcelain mortar. For each sample of ZnS:Al alloys, ground samples were prepared and used in deposition of the thin films. An Edwards Auto 306 Sputtering and Evaporation machine was used for the thin film deposition. Figure 4.1 shows Edwards Auto 306 Sputtering and Evaporation equipment

Fig. 4.1: Edwards Auto 306 Magnetron Sputtering and Evaporation equipment

4.1.4 Deposition of ZnS:Al Thin Films

The vacuum chamber of the vacuum coater was cleaned to remove any dust debris. Glass slides dimensions 38 mm long, 26 mm wide and 1 mm thick, were used as substrates. Glass substrates were then mounted on the substrate holder and 0.1g of each of the ZnS:Al alloy samples placed on the evaporation boat one at a time. The vacuum chamber was sealed and flushed with argon to remove any residual oxygen prior to deposition and pumped down to ultra - low pressure of 3.0×10^{-5} mbar at room temperature. The alloy sample in the tungsten evaporation boat was then heated to evaporate onto the glass substrates. Figure 4.2 shows schematic diagram showing evaporation chamber.

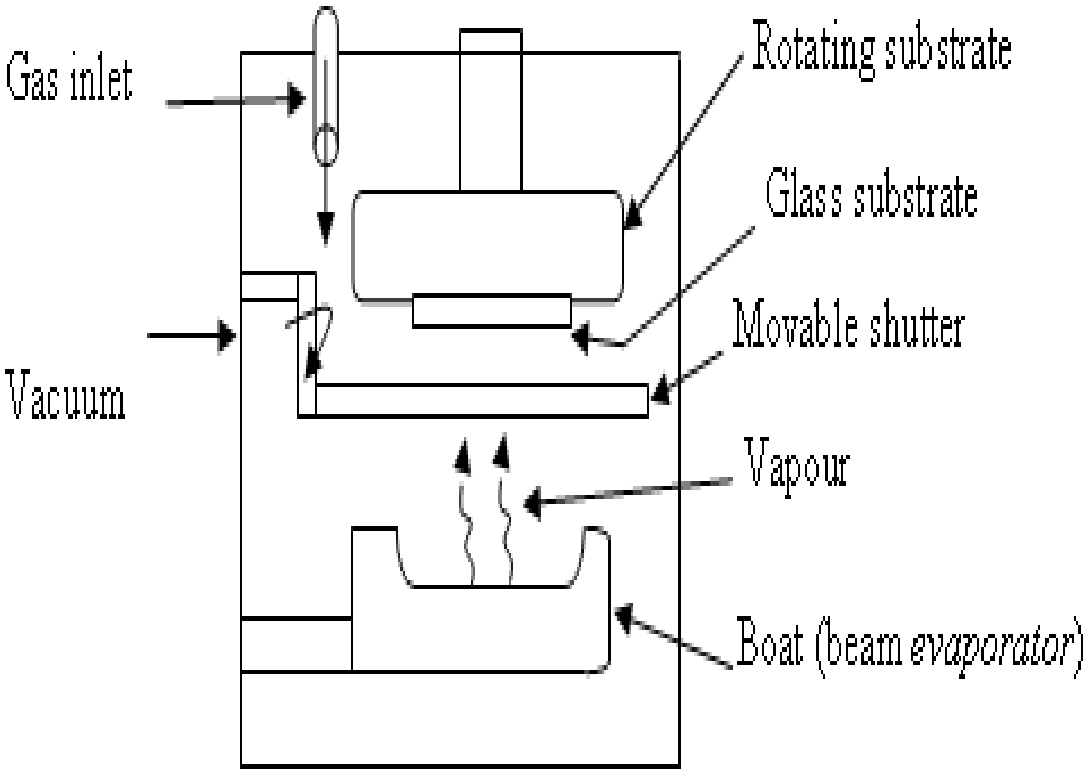

Fig. 4.2: Schematic diagram showing evaporation chamber for ZnS: Al thin films

Table 4.2: Summary of deposition parameters for ZnS:Al films

PARAMETER	VALUE
Deposition current	6A
Deposition time	60 seconds
Base Pressure	$3.0x10^{-5}$mbars
Mass of ZnS:Al samples	0.1g (0-10%)
Substrate Temperature	300K

4.2 Optical Characterization of Cu_2O and ZnS:Al Thin Films

Reflectance and transmittance of Cu_2O and ZnS:Al films were measured using optical spectrum analyzer. Reflectance and transmittance measurements for spectral range of 200-1200 nm were done with the aid of Solid Spec 3700 DUV Spectrophotometer machine. Figure 4.3 shows a photograph of Solid Spec 3700 DUV Spectrophotometer machine while figure 4.4 shows a schematic diagram for optical measurement. Absorbance of the Cu_2O and ZnS:Al films was calculated from transmittance and reflectance data using equation 3.2. (page 19)

The transmittance data for each sample of the thin films was simulated using scout software to determine optical constants such as absorption coefficient and refractive index.

Fig. 4.3: Solid Spec 3700 DUV Spectrophotometer

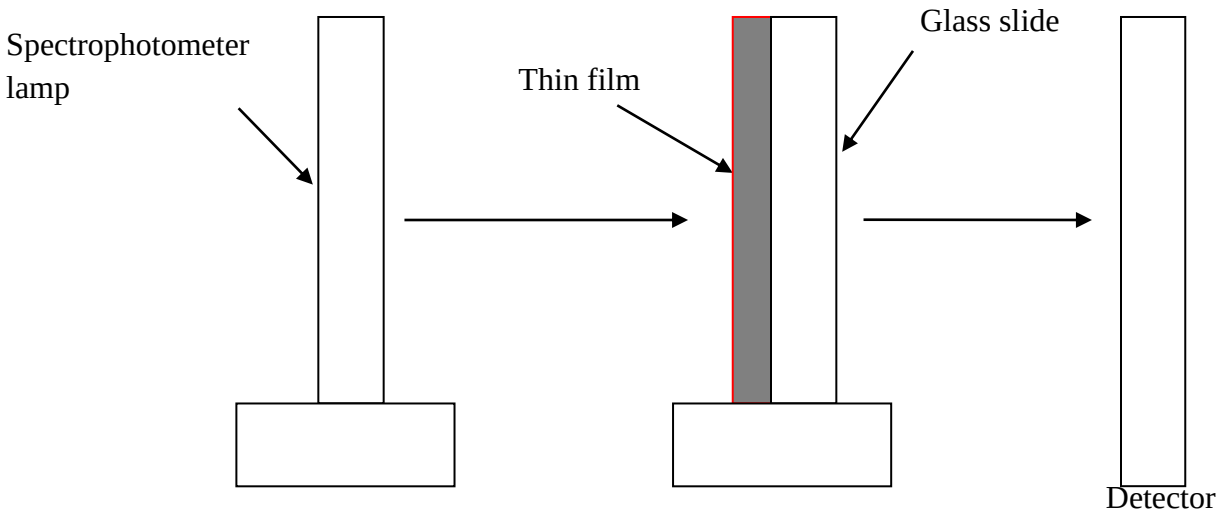

Fig. 4.4: Schematic diagram for optical measurements

The values of absorption coefficient were used to plot graphs of $(\propto hv)^2$ against photon energy, hv. The linear part of the graph was extended onto the energy axis and the optical band gap determined as shown in figure 4.5

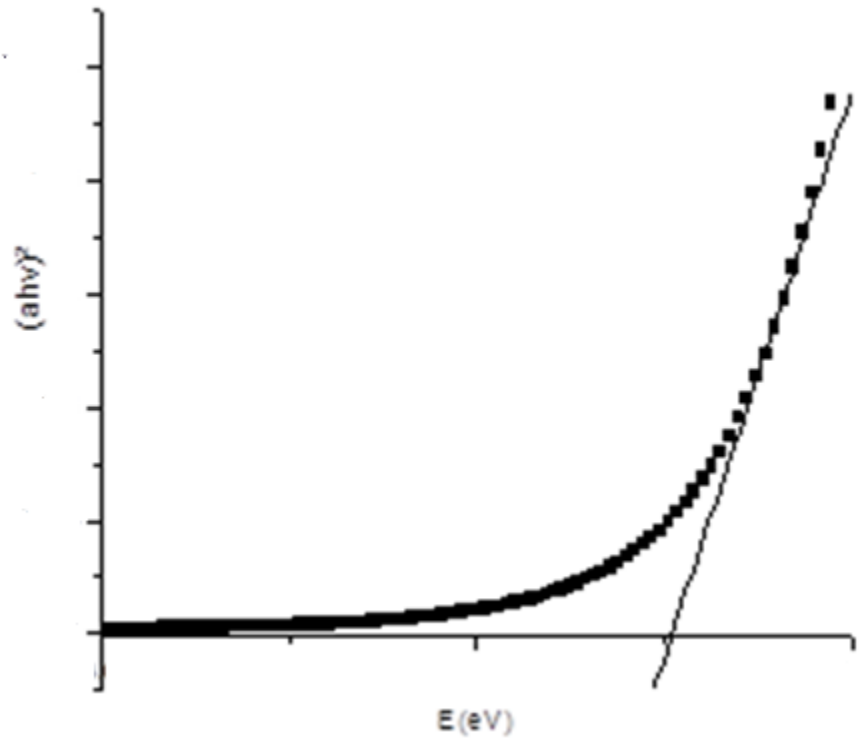

Fig. 4.5: Graph of $(\propto hv)^2$ vs energy (Ohring, 1995).

4.2.1 Thickness of Cu_2O Thin Films

Thickness of Cu_2O thin films was determined using Scout software by simulation of the transmittance data.

4.3 Electrical Characterization of Cu_2O and ZnS:Al Thin Films

Electrical characterization of Cu_2O and ZnS:Al thin films was done using four point probe technique. Figure 4.6 shows a schematic diagram of four point probe method for sheet resistance measurement while figure 4.7 is a set-up for electrical measurement. With linear geometry adopted, the four probe heads were connected to Keithley-2400 using conducting wires.

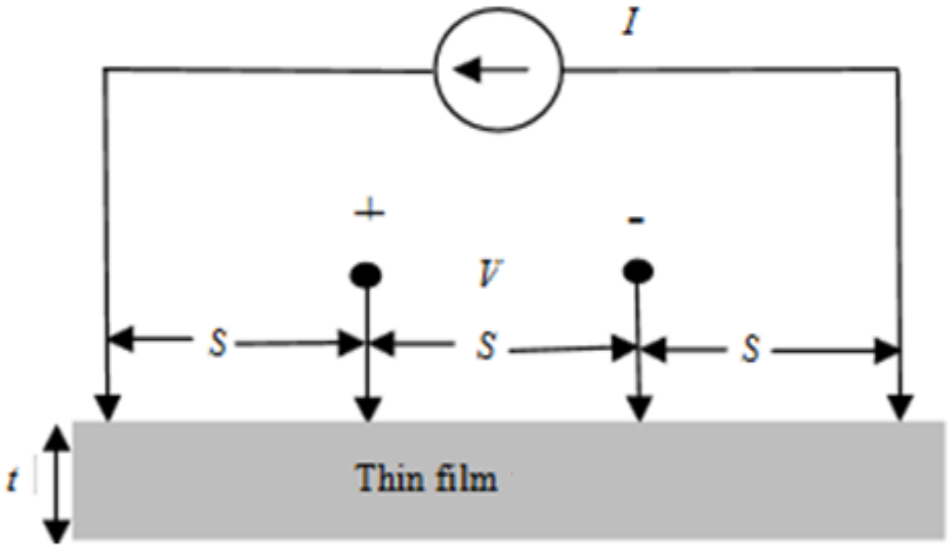

Fig. 4.6: Schematic diagram for four point probe method for sheet resistance measurement (Agumba, 2010)

With current sourced through the outer probes, the voltage was set across the inner probes. Sheet resistance of the Copper(I)Oxide and Aluminum doped ZnS films were calculated from the measured values of current and voltage. The resistivity of the films was calculated from the obtained values of sheet resistance using equation 3.17.

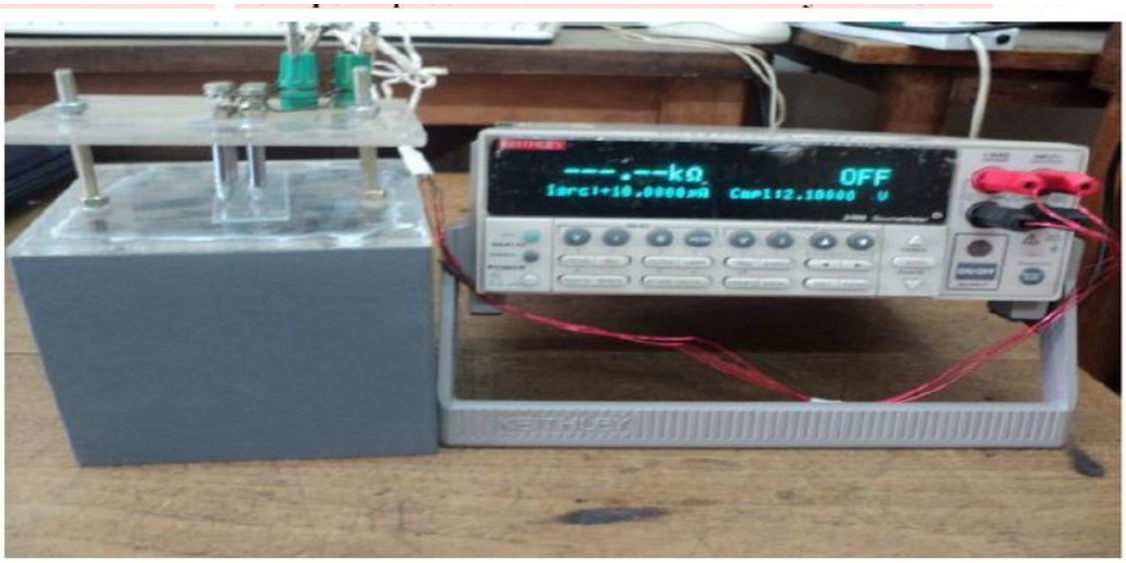

Fig. 4.7: Set-up for electrical characterization

4.4 Fabrication of Cu_2O- ZnS: Al p-n Junction

A glass slide of dimensions 2cm by 3cm to be used for fabrication of the solar cell was cut using a glass cutter. A solar cell with glass/ ZnS: Al /Cu_2O as in figure 4.8 was fabricated in steps. First, the n-type ZnS: Al film was deposited onto a glass substrate by evaporation method at pressure of $3x10^{-5}$ mbars. Then a p-type layer of Cu_2O film was deposited onto ZnS: Al on the same substrate by DC sputtering technique as described in section 4.1.1 and 4.1.3.

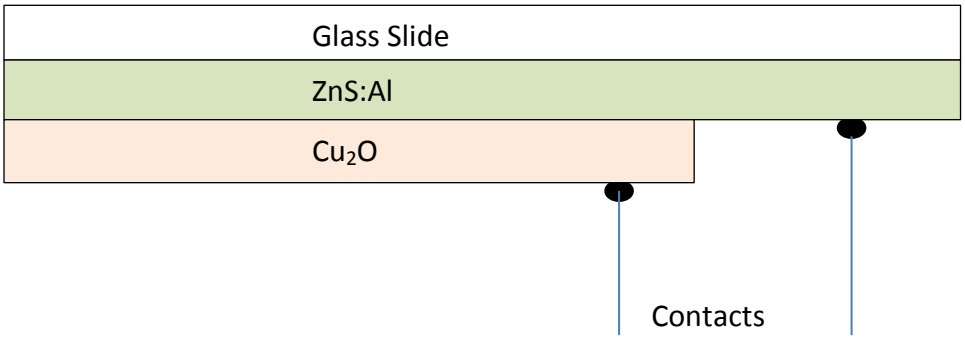

Fig. 4.8: Schematic diagram for Cu_2O- ZnS:Al solar cell

4.3 Characterization of Cu_2O- ZnS:Al p-n junction

The I-V data was measured using a solar simulator as shown in figure 4.9. The fan for the lamp of solar simulator was switched on. The power knob on the micro control was turned to give a power of 1000 W/m^2. The lamp was then switched on and remained on for 10 minutes before measurements were taken to ensure there was a steady radiation. I-V data was then obtained from the computer interfaced with Keithley 2400. The data obtained were used to plot I-V and P-V graphs as shown in figure 4.10. From the I-V and P-V graphs, I_{sc}, V_{oc}, I_{max} and V_{max} were determined. Fill factor and light conversion efficiency were calculated from the parameters obtained using equations 3.21 and 3.23, respectively.

Fig. 4.9: Set – up for I-V characterization

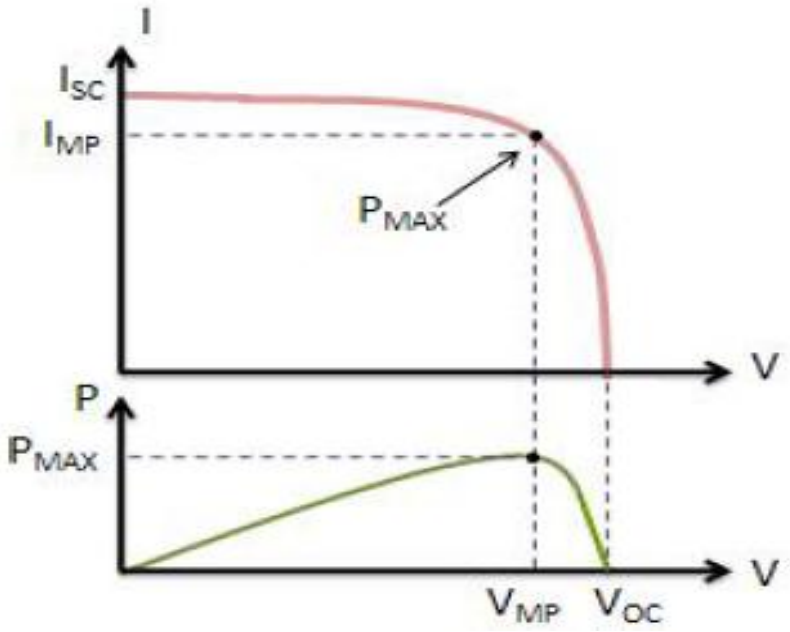

Fig. 4.10: I-V and P-V characteristics for a p-n junction under illumination, showing V_{max}, I_{max}, I_{sc}, V_{oc} (Lindholm *et al.*, 1979)

CHAPTER FIVE

RESULTS AND DISCUSSIONS

5.1 Optical Studies

Optical studies for both ZnS: Al and Cu_2O thin films were investigated separately and results obtained.

5.1.1 Optical Studies for ZnS: Al

Transmittance and reflectance for the films were measured directly and results obtained. The transmittance and reflectance data obtained were used to calculate absorbance of the thin films from equation 3.2. (page 19)

5.1.1.1 Transmittance and Reflectance

Figure 5.1 shows the graph of transmittance against wavelength for ZnS: Al thin films with varying doping concentrations. The average transmittance for undoped ZnS films was about 68% and this increased to about 85%, for 6% aluminium doping. The transmittance then decreased with further aluminium doping concentration. The increase in transmittance could be attributed to increased grain size and improved crystal structure while the decrease in transmittance at higher aluminium concentration may be attributed to lower grain size, formation of additional phases and higher defect density that lead to poor crystallinity of the layers. The increase of crystallinity may be due to incorporation of Al atoms in the Zn vacancies present in the samples. Above the 6% doping, there could be the presence of Al_2S_3 phase in the interstitial positions in ZnS lattice (Larena *et al.*, 2002). This result was in agreement with those reported by Prathap *et al.* (2008) and

Ngamani *et al*. (2012). Figure 5.2 shows a graph of average transmittance against wavelength.

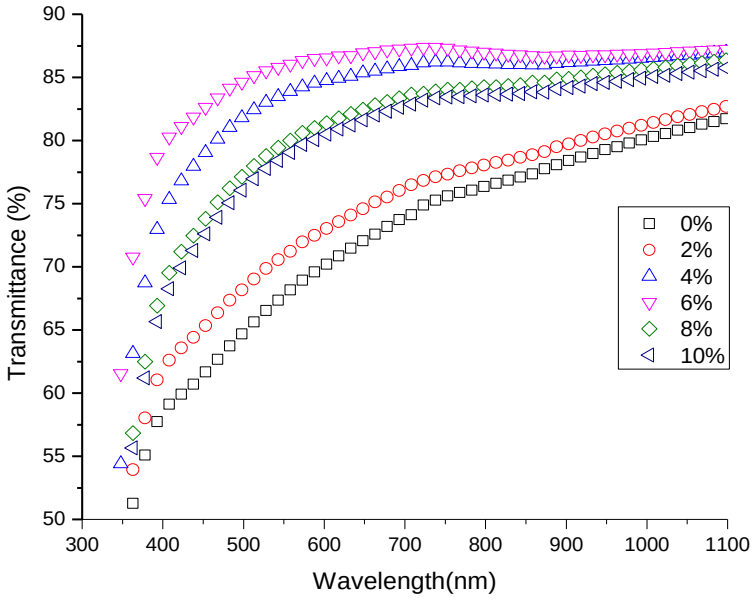

Fig. 5.1: Transmittance vs wavelength for ZnS:Al thin films at varying Al doping concentrations

Table 5.1: Average Transmittance for various Al. doping concentration of ZnS:Al thin films within VIS region

Al. doping concentration (%)	Average Transmittance (± 5 %)
0	68.2270
2	71.0892
4	82.7045
6	85.1420
8	80.7418
10	78.9129

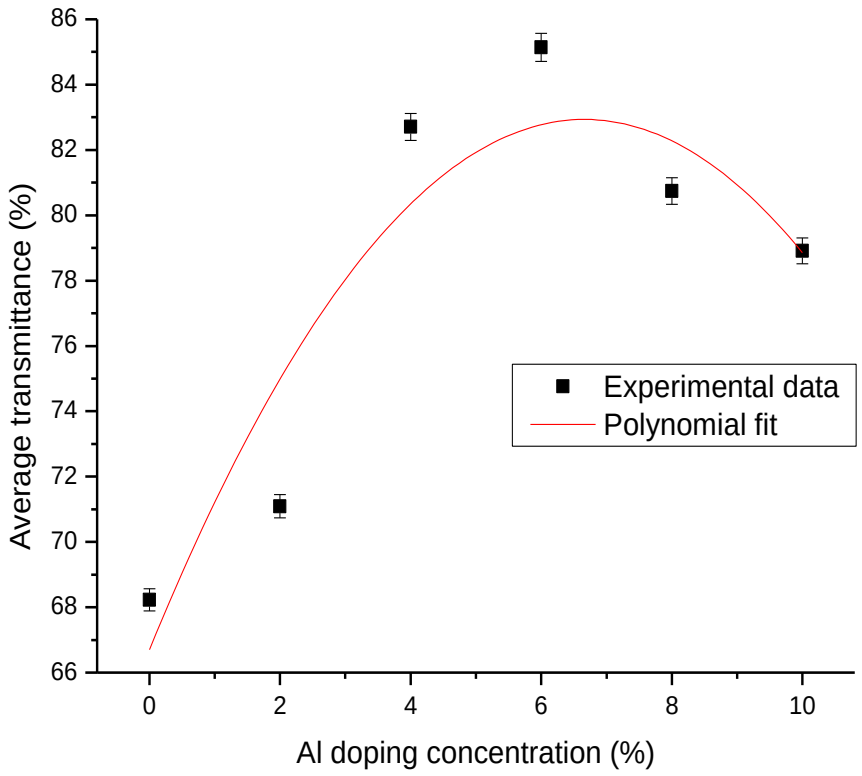

Fig. 5.2: Average transmittance at varying Al doping concentration for ZnS:Al thin films within VIS region. The graph shows both experimental and fitted data

All the ZnS: Al thin films showed low reflectance of below 25% as shown in figure 5.3. Reflectance of ZnS thin films decreased with aluminium doping concentration. The reduced reflectance makes ZnS: Al to be suitable for use as window layer for solar cell applications.

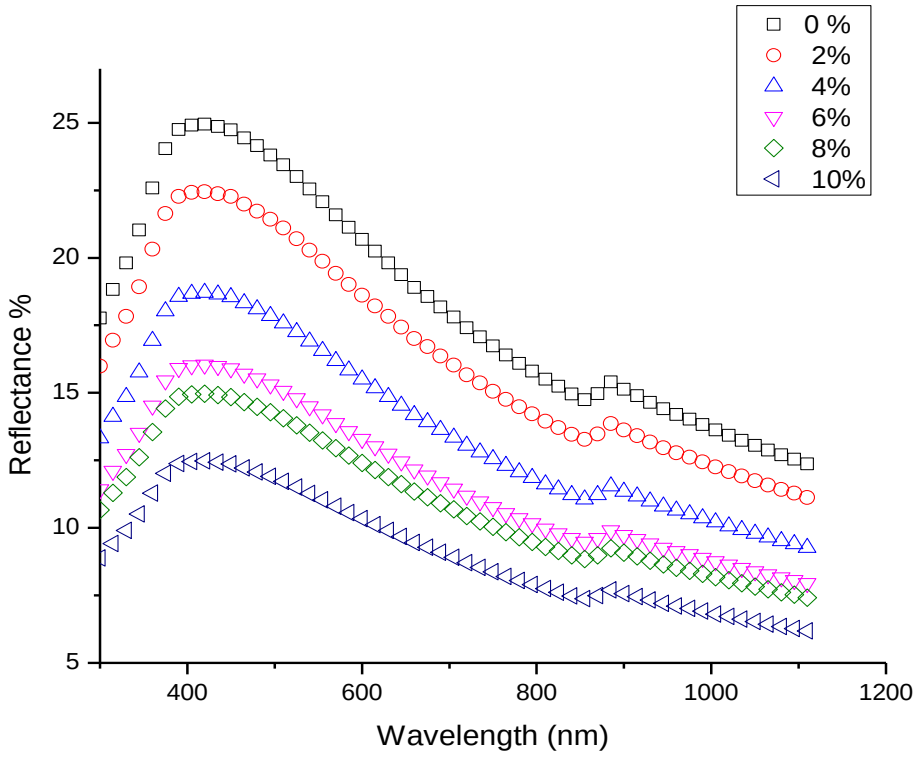

Fig. 5.3: Results showing reflectance vs wavelength for ZnS: Al thin films at varying doping concentrations.

5.1.1.2 Simulated and Experimental Graphs for ZnS:Al Thin Films

Transmittance data for ZnS:Al thin films were simulated using Scout software and graphs of experimental and simulated data plotted against wavelengths for various doping concentrations. The simulated curves fitted onto the experimental data as shown in the figure 5.4;

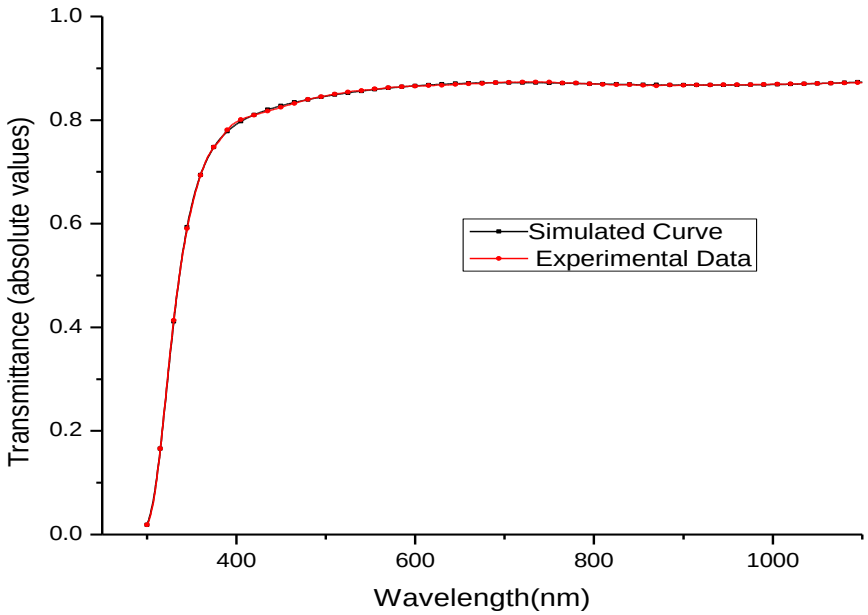

Fig. 5.4: Simulated and Experimental curves for ZnS:Al (6 % doping concentration)

5.1.1.3 Band Gap

The band gap of ZnS:Al thin film was obtained from the graph of $(\propto hv)^2$ against photon energy, hv. The linear part of the graph was extrapolated to meet the energy axis (at $(\propto hv)^2 = 0$). All the films deposited for various doping concentration showed direct band gap. The undoped ZnS had a wide band gap of 3.792eV. The band gap for the thin films decreased from 3.792 eV to 3.693 eV when the Al doping increased from 0% to 6% as shown in figure 5.5. This decrease in band gap could be attributed to formation of shallow or impurity levels in the band gap region. The formation of shallow level in the band gap region results in easy movement of the electrons from the top of valence band to bottom of conduction band. The result in this work is in agreement with results obtained by Hankare *et al.* (2005) for Pb-doped CdSe thin films. The marginal variations

in band gap between 0 % to 6 % Al doping concentration could be explained from the fact that the addition of Al atoms into ZnS lattice leads to decrease in the structural defects such as voids and dangling bonds, which may cause formation of unwanted localized states within the band gap, hence a decrease of structural disorder that reduces structural band tailing into the band gap region. (Smith, 1974). The band gaps from Tauc curve were almost equal to those calculated from Scout software as in table 5.2.

Table 5.2: Optical band gap of ZnS: Al thin films for varying Al doping concentrations

	Band Gap (eV)	
Al doping %	Experimental (± 0.05)	Computed (± 0.05)
0	3.792	3.789
2	3.790	3.791
4	3.759	3.761
6	3.693	3.692
8	3.702	3.701
10	3.722	3.720

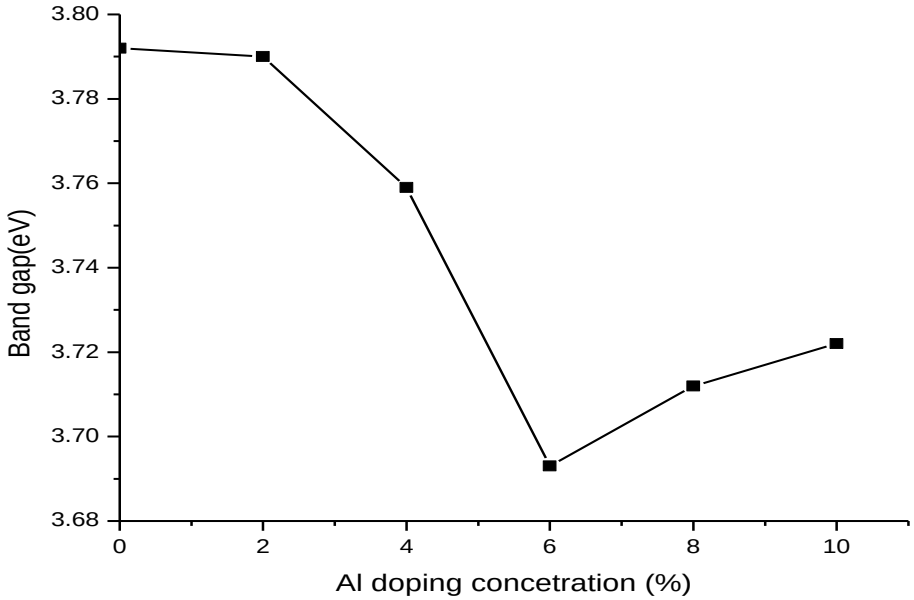

Fig. 5.5: Band gap of ZnS:Al thin films for varying Al doping concentrations

5.1.2 Optical Studies for Cu_2O

5.1.2.1 Transmittance and Reflectance

Transmission spectra showed that all the films had low transmission of below 45%. Transmission of Cu_2O films decreased from 43% to about 32% for films with thicknesses of 50 nm to 250 nm as shown in figure 5.6. This decrease in transmittance can be attributed to decrease in transparency of the film as the film thickness increases. Figure 5.8 shows absorption of Cu_2O films for various thicknesses. All the films showed high absorption of above 50% within the visible region. Absorption of Cu_2O thin films increased with thickness, with highest absorption of about 60% for about 200 nm film thickness as shown in figure 5.9. This increase in optical absorption of Cu_2O thin films could be attributed to increase in absorption sites as the film thickness increased. Table 5.3 shows average absorption for various thicknesses of Cu_2O thin films. All the films showed low reflectance of below 35%. Reflectance decreased with increased thickness from 32% to about 23% for film thicknesses of 50 nm to250nm.

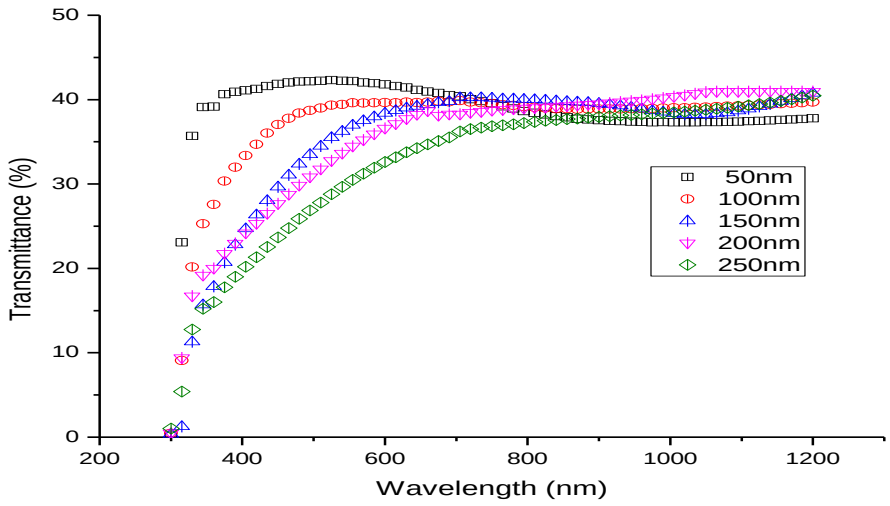

Fig. 5.6: Transmission spectra for Cu2O thin films at varying film thicknesses

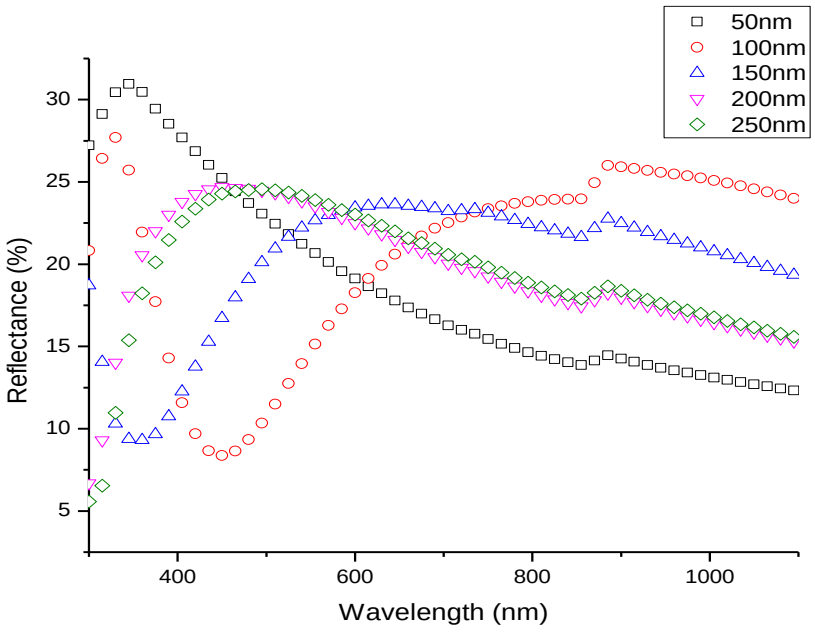

Fig. 5.7: Reflectance vs wavelength for Cu_2O thin films at varying thicknesses

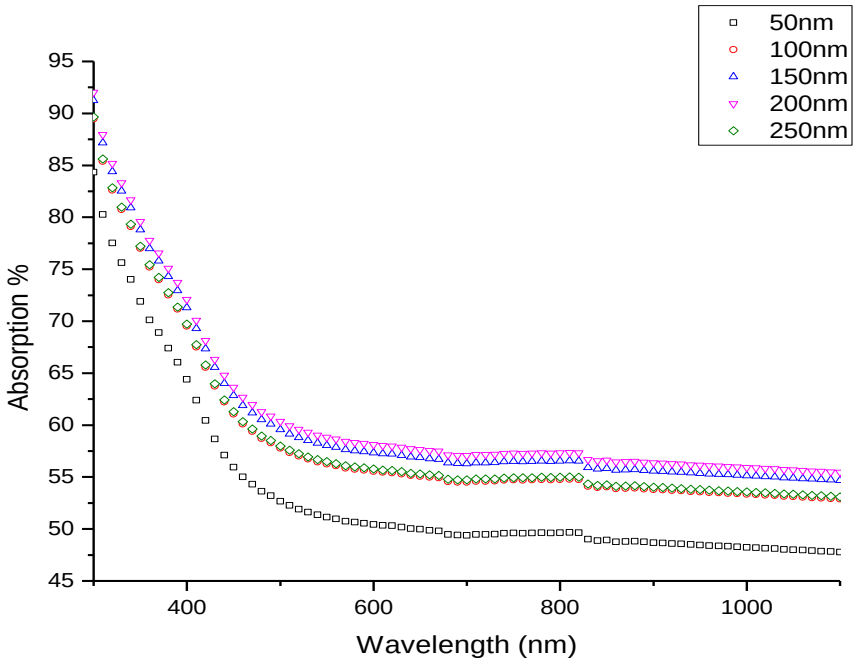

Fig. 5.8: Absorption Spectra for Cu_2O thin films at varying film thickness

Table 5.3: Average Absorption of Cu_2O thin films within VIS region

Thickness of Cu_2O ($\pm$5nm)	Average absorbance (%)
50	52.6049
100	57.7154
150	59.5019
200	60.2888
250	57.9341

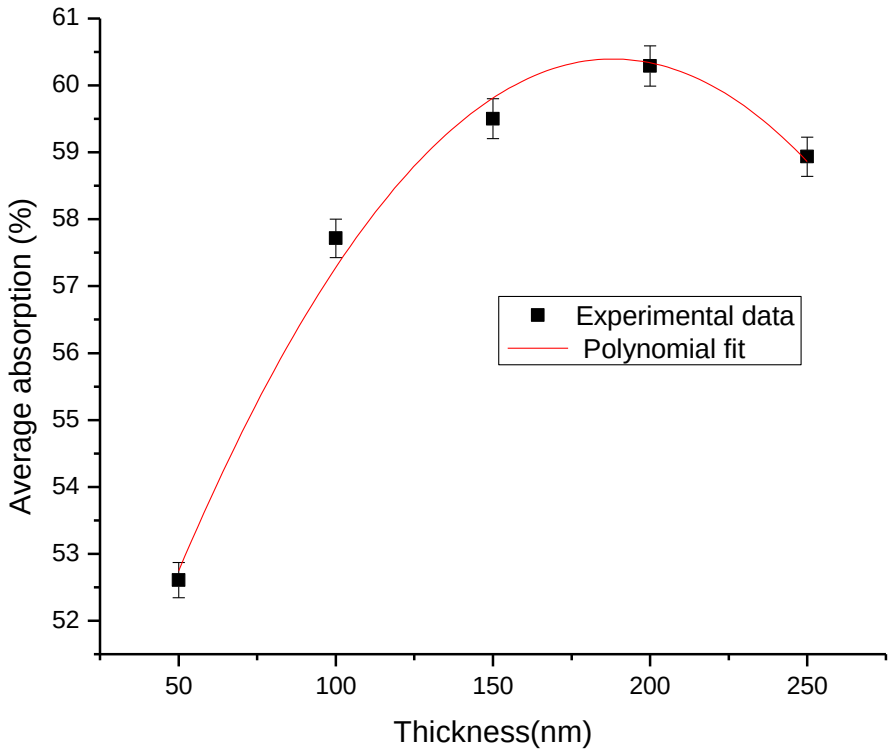

Fig. 5.9: Average absorption versus thickness for Cu2O thin films within VIS region

5.1.2.2 Simulated and Experimental Graphs for Cu_2O Thin Films

Transmittance data for Cu_2O thin films were simulated using Scout software and graphs of experimental and simulated data plotted against wavelengths for various thicknesses. The simulated curves fitted onto the experimental data as shown in the figure 5.10;

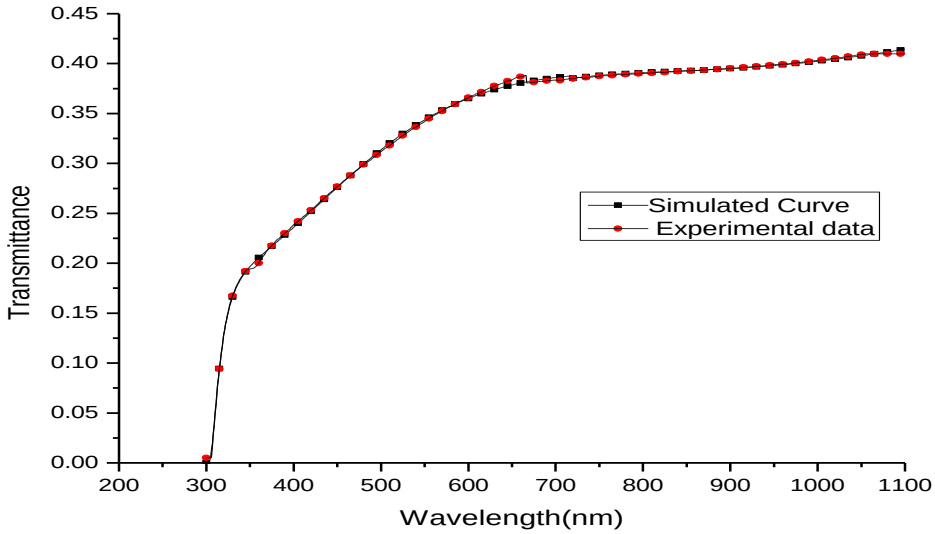

Fig. 5.10: Simulated and Experimental curves for Cu_2O thin films (200nm)

5.1.2.3 Band Gap

The band gap of Cu_2O thin films was obtained by plotting a graphs of $(\propto hv)^2$ against photon energy, hv. All the films showed direct band gaps. The Cu_2O band gap decreased from about 2.452eV to about 2.402eV for film thicknesses range 50 nm to 250nm. Table 5.4 shows the optical band gap for the thin films both from Tauc curves and calculated from Scout software. The calculated values of band gap were almost equal to those obtained the from graph. Figure 5.11 shows a graph of band gap for Cu_2O thin films of varying thickness. The values of band gaps obtained in this work were in the range of

those obtained by Mugwang'a *et al.* (2012). The decrease in band gap could be attributed to the presence of unstructured defects which decreased the density of localized states in the band gap region and consequently decrease in energy (Sengupta *et al.* 2011). The low band gap of Cu_2O thin films makes it suitable as an absorber layer in solar cell applications.

Table 5.4: Optical band gap of Cu_2O for various film thicknesses

Film thickness (nm) (± 5)	Band Gap from Tauc Curve (eV) (± 0.005)	Band Gap from Scouts (eV) (± 0.005)
50	2.452	2.456
100	2.447	2.448
150	2.432	2.438
200	2.418	2.421
250	2.410	2.411

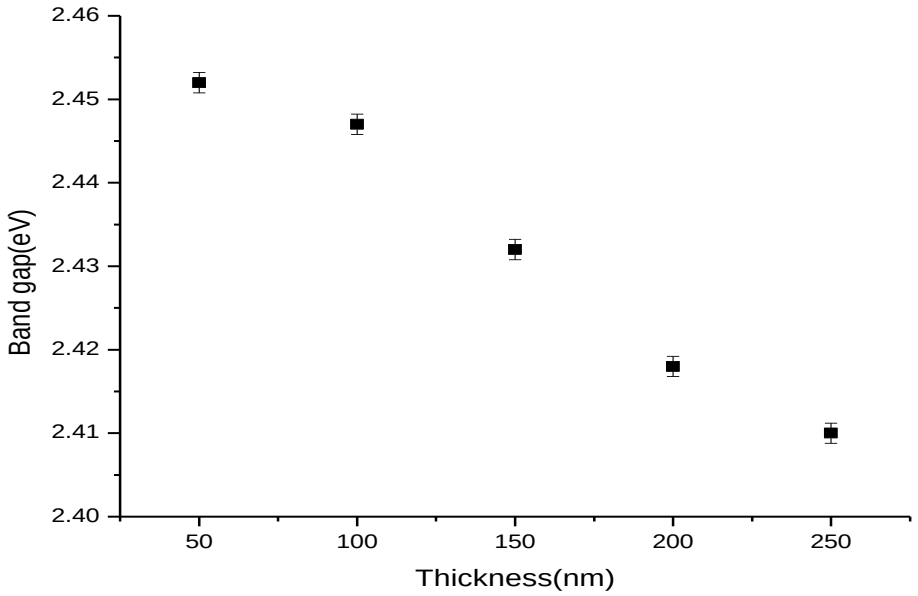

Fig. 5.11: Variation of band gap with film thickness for Cu2O thin films

5.2 Electrical Properties

5.2.1 Resistivity of ZnS: Al Thin Films

Sheet resistance of ZnS:Al thin films were determined using four point probe method. The resistivity of the films was then calculated from equation 3.17 (page 25). The electrical resistivity of ZnS:Al thin films decreased from about 1.54 x 10^5 Ωcm for undoped ZnS thin film to about 69 Ωcm for 6 % Al concentration then increased to about 4.55 x 10^5 Ωcm with further increase in doping concentration of 10 %. as shown in figure 5.12. The decrease in resistivity at lower doping levels could be attributed to introduction of extra charge carriers into the ZnS lattice. The further increase in resistivity could be attributed to the fact that extra aluminium atoms occupy spaces between the atoms in the ZnS lattice and formation of Al_2S_3 at the grain boundaries (Cosement *et al.*, 1985).

Table 5.5: Resistivity of ZnS: Al for various Al. concentration

Al doping %	Resistance ($\times 10^9 \Omega$) (± 0.005)	Resistivity ($\times 10^5 \Omega$cm) (± 0.005)
0	1.7046	1.54512
2	0.6792	0.61562
4	0.1750	0.15858
6	0.0008	0.00069
8	0.0651	0.05965
10	0.5026	0.45556

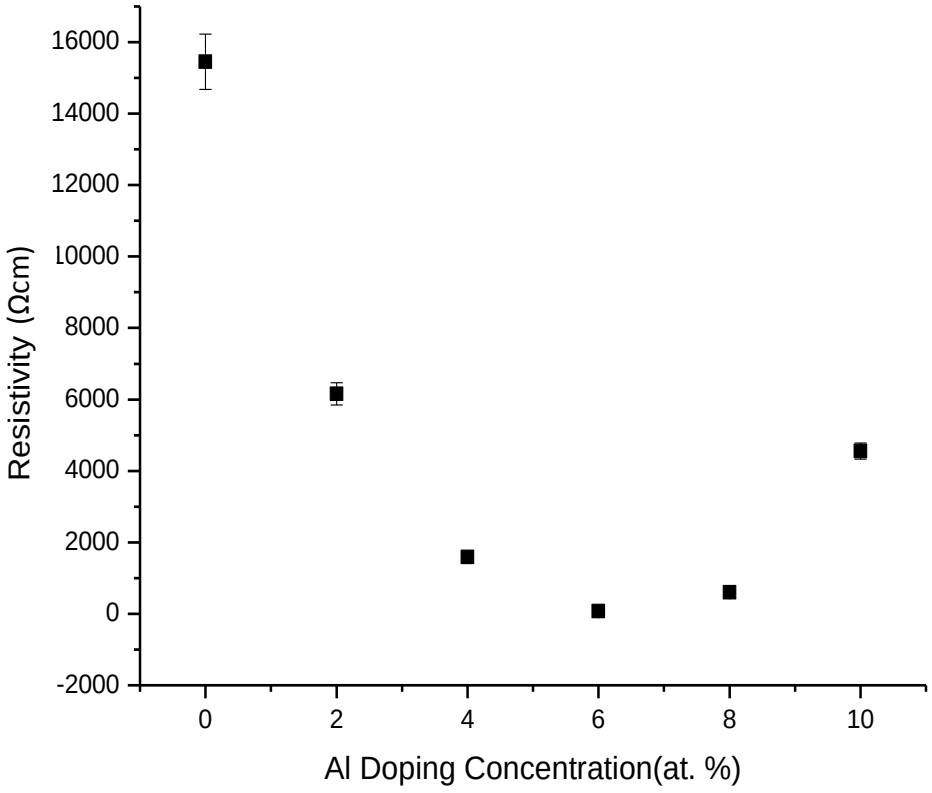

Fig. 5.12: Resistivity of ZnS: Al thin film at varying Al concentration

5.2.2 Resistivity of Cu_2O Thin Films

Resistivity of Cu_2O thin films increased from 7 Ωcm to 53 Ωcm with increase in thicknesses from 50 nm to 250 nm. Figure 5.13 shows variation of resistivity with thickness for Cu_2O thin films. The increase in resistivity of Cu_2O thin films with increase in thickness could be attributed to increase in the vibration of atoms as a result of increased density of the films which inhibit the movement of the charge carriers.

Table 5.6: Resistivity of Cu_2O thin films for various thicknesses

Thickness(±5nm)	Resistance($\times 10^4\Omega$)	Resistivity (Ωcm)
50	302	7.1171
100	354	16.0433
150	386	25.8904
200	432	39.5480
250	480	53.5139

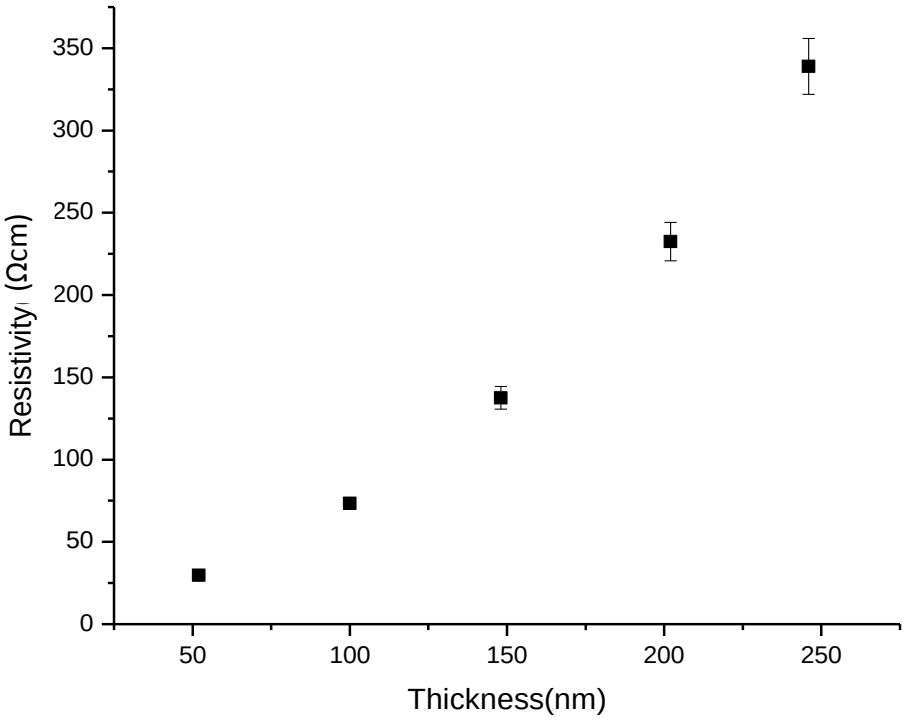

Fig. 5.13: Resistivity of Cu_2O thin film at varying film thickness

5.3 Optimized Parameters of Cu_2O and ZnS: Al Thin films

Cu_2O and ZnS: Al thin films with the best optical and electrical properties were chosen for fabrication of Cu_2O - ZnS: Al p-n junction. The summary of optimized parameters for Cu_2O and ZnS: Al thin films are given in tables 5.7 and 5.8 respectively.

Table 5.7: Summary of optimized parameters for Cu_2O thin films

PARAMETER	VALUE
Sputter power	200 W
Band gap energy	2.421 eV
Resistivity	39.44 Ωcm
Optical absorption within visible region	60.288 %

The optimized Cu_2O thin films had a high absorption of about 60 % and low band gap of 2.421 eV. This high absorption and low band gap makes it suitable for absorber layer for solar cell applications.

6 % Al doped ZnS was chosen as a window layer for fabricating Cu_2O - ZnS:Al p-n junction because it had the highest transmittance within the visible region and relatively low electrical resistivity. This high transmittance makes it suitable for use as window layer in a solar cell.

Table 5.8: Summary of optimized parameters for ZnS:Al thin films

PARAMETER	VALUE
Dopant concentration	6 %
Band gap energy	3.692 eV
Resistivity	69 Ωcm
Optical transmission within visible region	85.1420 %

5.4 Solar Cell Characteristics

I-V and P-V characteristics of Cu_2O - ZnS:Al solar cell are shown in figure 5.14. From the I-V and P-V curves, short circuit current, $I_{sc,}$ open circuit voltage, Voc, current at maximum power output, I_{max} and voltage at maximum power output, $V_{max,}$ were obtained at input power of 1000 W/m^2. The maximum power output was determined to be 3.725mW/m^2. Fill factor, FF and conversion efficiency of the fabricated solar cell were determined using equations 3.21 and 3.23 respectively. Table 5.9 shows Cu_2O - ZnS:Al solar cell parameters

Table 5.9: Cu_2O - ZnS: Al solar cell parameters

PARAMETER	VALUE
Short Circuit Current, I_{sc}	$1.0x10^{-2}$A
Open Circuit Voltage, Voc	592 mV
Maximum Current, I_{max}	9.042 mA
Maximum Voltage, V_{max}	412m V
Fill Factor, FF	0.62%
Conversion Efficiency	0.629

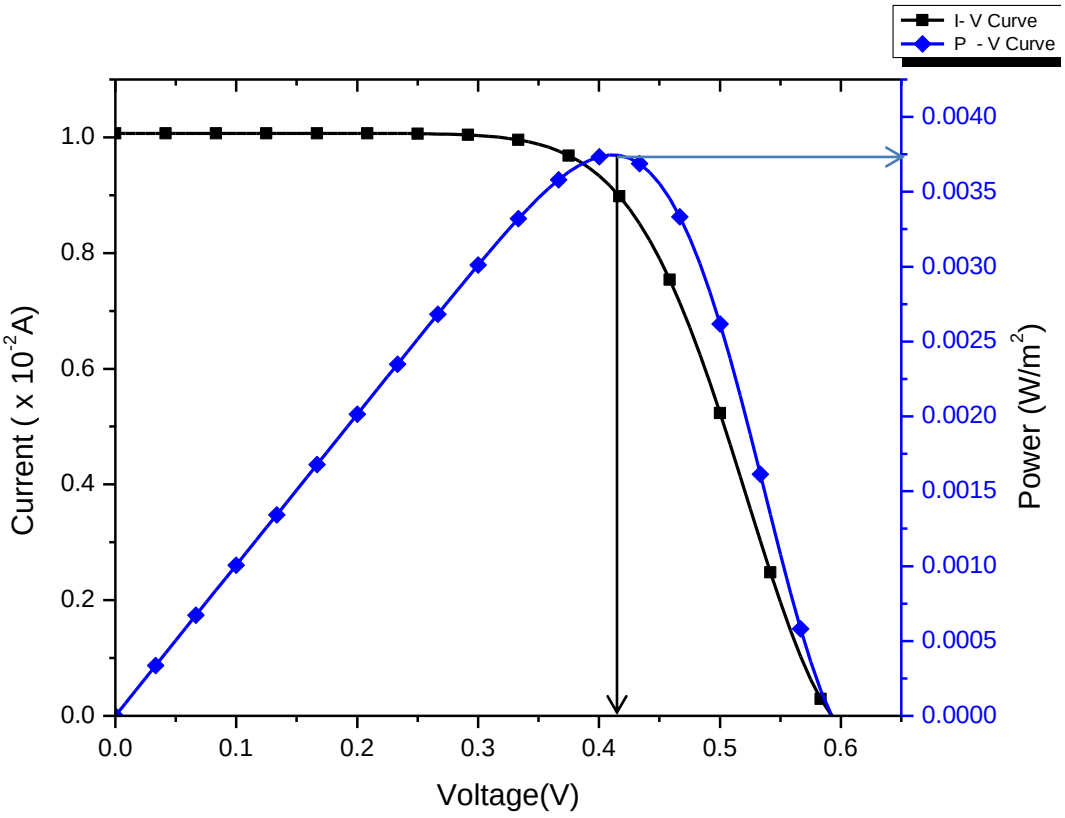

Fig. 5.14: I-V and P-V characteristics for Cu_2O – ZnS: Al p-n junction under illumination, showing V_{max}, I_{max}, I_{sc}, V_{oc}.

Kidowaki *et al.,* (2012) obtained a conversion efficiency of 1.8 x 10^{-6}%, in Cu_2O/C_{60} solar cell using Cu_2O as absorber layer, with FF of 0.25, Isc of 0.18×10^{-3} $mAcm^{-2}$ and Voc of 0.04 V. In this work Cu_2O – ZnS: Al p-n junction was fabricated with and a relatively low efficiency of 0.62% obtained. This may be attributed to the effect of the morphology of the glass used as the substrate.

CHAPTER SIX

CONCLUSIONS AND RECOMMENDATIONS

6.1 Conclusions

Cu_2O and ZnS: Al thin films were deposited successfully by DC reactive sputtering and evaporation methods respectively. Transmission of Cu_2O films decreased from 43% to about 32% for films with thicknesses 50 nm to 250 nm. All the Cu_2O films showed high absorption of above 50% within the visible region. Absorption of Cu_2O films increased with thickness, with highest absorption of about 60% for about 200 nm film thickness. The band gap of Cu_2O decreased from 2.452 eV to 2.402 eV for film thicknesses 50 nm to 250 nm. The average transmittance of undoped ZnS films was about 68% and this increased to about 85% for the thin film of Al. doping of 6%.

From the optical measurements it was noted that Al doping effectively increased the optical transmission of ZnS thin films. ZnS:Al thin film had the highest transmission of about 85% at 6% Al concentration. Doping also had an effect of decreasing the optical band gap of ZnS thin films from 3.792 eV to 3.693 eV. The resistivity decreased greatly as a result of doping from 1.54×10^5 Ωcm for undoped ZnS thin film to 69 Ωcm for Al doping of 6 at.% due to introduction of extra charge carriers into the ZnS lattice.

Resistivity of Cu_2O films increased from about 7 Ωcm to 53 Ωcm with increase in thicknesses from 50 nm to250 nm. The electrical resistivity of ZnS: Al thin films decreased from 1.54×10^5 Ωcm for undoped ZnS thin film to 69 Ωcm for Al

concentration of 6 % then increased to 4.55 x 10^5 Ωcm with further increase in doping concentration of 10 %.

Cu_2O thin film of thickness 200nm and ZnS: Al of Al doping of 6 % thin film were used to fabricate Cu_2O - ZnS: Al solar cell. The short circuit current of the solar cell was $1.0x10^{-2}$A and open circuit voltage was 0.592 V. Voltage and current at maximum power i.e. I_{MAX} and V_{MAX} obtained were 9.042mA and 0.412 V respectively, giving a maximum power of 3.725mW/m^2. The Fill factor of the solar cell fabricated was determined to be 0.629 and conversion efficiency was 0.62%.

6.2 Recommendations

Thin films of Cu_2O and ZnS: Al are therefore suitable materials for solar cell applications. Cu_2O has low bad gap and high absorption hence suitable for use as an absorber layer while ZnS: Al has wide band gap and high transmission within VIS region hence suitable as a window layer.

Very little research has been done on ZnS: Al as a window layer solar cells, therefore further studies should be done on other ZnS:Al based cells, with ZnS: Al as n -layer.

Finally, structural analyses need to be done to investigate the effect of Al doping on the crystal structure of ZnS thin films. In addition, studies on the morphology of the glass used for the slides and its effects on the efficiency of the solar cell also need to be done.

REFERENCES

Agumba, J. O. (2010). Design and fabrication of a simple four point probe system for electrical characterization of thin films. *M.Sc. Thesis*, Department of Physics. Kenyatta University.

Balzani, V. and Armaroli, N. (2010). Energy for a sustainable world: from the oil age to a sun-powered future. John Wiley and Sons.

Chan, J., and Spring (1994). Four-point probe manual. *EECS Microfabrication Technology*. University of Carlifornia.

Cossement, D., and Streydio, J. M. (1985). Fabrication of ZnO polycrystalline layers by chemical spray. *Journal of Crystal Growth*, *72*(1-2), 57-60.

Eduardo, L. (1994). Solar Electricity: Engineering of Photovoltaic Systems. Progensa. ISBN 84-86505-55-0.

Green, M. A. (1982). Solar cells: operating principles, technology, and system applications. *Englewood Cliffs*, NJ, Prentice-Hall, 288 p.

Green, M. A. (2004). Recent developments in photovoltaics. *Solar energy*, *76*(1-3), 3-8.

Gunther, K. G. (1966). The use of thin films in physical investigations.

Hankare, P.P., Delekar, S.D., Chate, P.A., Sabane, S.D.,Garadkar, K.M. and Bhuse, V.M. (2005). A Novel Route to Synthesize Cd_{1-x} Pb_xSe Thin Films from Solution Phase. *Semiconductor science technology*, 20:257.

Izaki, M., Mizuno, K. T., Shinagawa, T., Inaba, M., and Tasaka, A. (2006). Photochemical construction of photovoltaic device composed of p-copper (I) oxide and n-zinc oxide. *Journal of the Electrochemical Society*, 153(9), C668-C672.

Jiang, P., Jie, J., Yu, Y., Wang, Z., Xie, C., Zhang, X., and Luo, L. (2012). Aluminium-doped n-type ZnS nanowires as high-performance UV and humidity sensors. *Journal of Materials Chemistry*, *22*(14), 6856-6861.

Kemell, M. (2003). Electrodeposition of CuInSe_2 and doped ZnO thin films for solar cell. PhD. Thesis University of Helnsiki, Faculty of Science, Finland.

Kidowaki, H., Oku T. and Akiyama, T. (2012). Fabrication and Evaluation of CuO/ZnO Heterostructures for Photoelectric conversion. *International Journal for Research and Reviews in Applied Science*, 13 (1):67-72.

Kittel, C. (1995). Introduction to Solid State Physics. 7th ed. John Wiley and Sons, New York ISBN 0-471-11181-3.

Kobayashi, H.; Nakamura, T. and Takahash, N. (2007). Preparation of Cu2O Films on MgO (110) Substrate by Means of Halide Chemical Vapor Deposition under Atmospheric Pressure.Materials Chemistry and Physics, 106 (2-3), (December 2007), pp. 292, ISSN 0254-0584.

Kushkul, E.N. (2001). The effect of ZnS thickness on the p-n junction. *M. Sc. Thesis*, University of Mustansiriyah, Baghdad, Iraq.

Kylner A. (1999). Effect of impurities in the CdS buffer layer on the performance of the $Cu(In,Ga)Se_2$ thin film solar cell. *Journal of Applied Physics,* 85: 6858-6865.

Larena, A., Millán, F., Pérez, G., and Pinto, G. (2002). Effect of surface roughness on the optical properties of multilayer polymer films. *Applied Surface Science*, *187*(3-4), 339-346.

Lindholm, F. A., Fossum, J. G., and Burgess, E. L. (1979). Application of the superposition principle to solar-cell analysis. *IEEE Transactions on Electron Devices*, *26*(3), 165-171.

Lothian, G.F. (1958). Absorption Spectrophotometry, 2nd edn, Hisher and Watts Ltd London, 19:20.

Maissel, L. I. (1966). Physics of thin films, G. Hasi and R.E. Tun (eds) vol. 3, Academic Press Inc. New York, 61.

Markvart, T. (1998). Solar Cells: Materials, Manufacture and operation. John Wiley and Sons. New York.

Matsunami, N., Yamamura, Y., Itikawa, Y., Itoh, N., Kazumata, Y., Miyagawa, S., and Shimizu, R. (1981). A semiempirical formula for the energy dependence of the sputtering yield. *Radiation Effects*, 57(1-2), 15-21.

Mehta, S. K., Kumar, S., Chaudhary, S., and Bhasin, K. K. (2010). Nucleation and growth of surfactant-passivated CdS and HgS nanoparticles: time-dependent absorption and luminescence profiles. *Nanoscale*, *2*(1), 145-152.

Meinel, A. B., and Meinel, M. P. (1976). Applied Solar Energy, An Introduction Addison-Wesley. *Reading MP*.

Mugwang'a, F. K., Karimi, P. K., Njoroge, W. K., Omayio, O., and Waita, S. (2012). Optical characterization of copper oxide thin films prepared by reactive dc magnetron sputtering for solar cell applications.

Nagamani, K., Prathap, P., Lingappa, Y., Miles, R. W., and Reddy, K. R. (2012). Properties of Al-doped ZnS films grown by chemical bath deposition. Physics Procedia, 25:137-142.

Ogwu, A. A., Bouquerel, E., Ademosu, O., Moh, S., Crossan, E., and Placido, F.(2005). An investigation of the surface energy and optical transmittance of copper oxide thin films prepared by reactive magnetron sputtering Thin Film Centre, Electronic Engineering and Physics Division, Acta Materialia 53 :5151–5159.

Ohring, M. (1992). Thin film materials science, United Kingdom, London.

Ohring, M. (1995). Materials science of thin films, United Kingdom, London.

Ohtomo, A., and Tsukazaki, A. (2005). Pulsed laser deposition of thin films and superlattices based on ZnO. *Semiconductor science and technology*, *20*(4), S1.

Oladeji, I. O., and Chow, L. (2005). Synthesis and processing of CdS/ZnS multilayer films for solar cell application. *Thin Solid Films*, *474*(1-2), 77-83.

O'Leary, S. K., Johnson, S. R., and Lim, P. K. (1997). The relationship between the distribution of electronic states and the optical absorption spectrum of an amorphous semiconductor: An empirical analysis. *Journal of applied physics*, *82*(7), 3334-3340.

Olsen, L. C., Bohara, R. C., and Urie, M. W. (1979). Explanation for low-efficiency Cu2O Schottky-barrier solar cells. *Applied physics letters*, *34***(**1), 47-49.

Pan, J., Yang, C., and Gao, Y. (2016). Investigations of cuprous oxide and cupric oxide thin films by controlling the deposition atmosphere in the reactive sputtering method. *Sens. Mater.*, *28*(7), 817-824.

Pankove, J. I. (1975). Optical processes in semiconductors. Courier Corporation.

Papadimitriou, L., Economou, N. A., and Trivich, D. (1981). Heterojunction solar cells on cuprous oxide. *Solar cells*, ***3***(1), 73-80.

Papadimitropoulos, G., Vourdas, N., Vamvakas, V. E., and Davazoglou, D. (2005). Deposition and characterization of copper oxide thin films. In *journal of physics: conference series* (Vol. 10, No. 1, p. 182). IOP Publishing.

Pethe, S. (2004). Optimization of the two stage process for Cu (In, Ga) Se_2 solar cells.

Prathap, P., Revathi, N., Subbaiah, Y. V., Reddy, K. R., and Miles, R. W. (2008). Preparation and characterization of transparent conducting ZnS: Al films. *Solid State Sciences*, *11*(1), 224-232.

Rai, B. P. (1988). Cu2O solar cells: a review. *Solar cells*, *25*(3), 265-272.

Rakhshani, A. E. (1986). Preparation, Characteristics And Photovoltaic Properties of Cuprous-Oxide – A review. *Solid-State Electronics*, 29: 7-17.

Robert, W. M., Guillaume, Z. and Ian, F. (2007). Inorganic photovoltaic cells. *Northumbria Photovoltaics Applications Centre conference*, 10: 11-20.

Robertson, J., Peacock, P. W., Towler, M. D., and Needs, R. (2002). Electronic structure of p-type conducting transparent oxides. *Thin Solid Films*, *411*(1), 96-100.

Sengupta, J., Sahoo, R. K., Bardhan, K. K., and Mukherjee, C. D. (2011). Influence of annealing temperature on the structural, topographical and optical properties of sol–gel derived ZnO thin films. *Materials Letters*, *65*(17-18), 2572-2574.

Serhan A. A. (2005). Preparation and Characterization of Chlorine doped Cadmium Sulphide (CdS:Cl) thin films and their applications in solar cells. Msc Thesis. King Saud University, College of Science: Department of Physics and Astronomy.

Sharma, S. P. (1979). Adsorption of water on copper and cuprous oxide. *Journal of Vacuum Science and Technology*, *16*(5), 1557-1559.

Smith, R. A. (1974). Semiconductors, (Cambridge University, Cambridge, 1978). *Google Scholar*, 72.

Stone, J. L. (1993). Photovoltaics: Unlimited electrical energy from the sun. *Physics Today; (United States)*, *46*(9).

Sze, S. M. (2008). Semiconductor Devices: Physics and Technology. John Wiley and Sons, New York.

Sze, S. M. (1981) Physics of Semiconductor Devices, John Wiley and Sons, New York. *Google Scholar*.

Tsubomura, H., and Kobayashi, H. (1993). Solar cells. *Critical Reviews in Solid State and Material Sciences*, *18*(3), 261-326.

Wielder, S. (1982). An Introduction to solar energy for scientists and engineers. *John Willy and Sons*.

Würfel, U., Cuevas, A., and Würfel, P. (2015). Charge carrier separation in solar cells. *IEEE Journal of Photovoltaics*, *5*(1), 461-469.